SELF-ASSEMBLY OF LITHOGRAPHICALLY

PATTERNED MICROPOLYHEDRA

By
Shivendra Pandey

A dissertation submitted to The Johns Hopkins University in conformity with the requirements for the degree of Doctor of Philosophy

Baltimore, Maryland
September 2014

Abstract

Nature utilizes self-assembly to create structures at a range of length scales. In addition, a variety of biological nanostructures such as viruses have polyhedral geometries and are formed using highly parallel assembly processes. In contrast, it is very challenging to assemble synthetic polyhedra with patterned surfaces at sub-millimeter scales using conventional engineering practices. Inspired by natural fabrication, this thesis is focused on understanding how to assemble such patterned micropolyhedra using both modeling and experiments.

Specifically, my work is focused on the development of model polyhedral systems using lithography and self-assembly techniques, demonstrating material versatility and uncovering underlying geometric design rules using mathematical tools. I have investigated an algorithmic approach to self-assemble complex polyhedra such as truncated octahedra. Here, new geometric design rules related to compactness of the precursor nets and pathways were uncovered. I also have studied the influence of pathways and degrees of freedom of intermediates in the assembly of polyhedral isomers and these findings have been compared to geometric models of molecular isomers notably cyclohexane.

In addition to a fundamental understanding of self-assembly of polyhedra, I have also explored applications of micropolyhedra. Importantly, I studied a molding process to enhance material versatility and fabricate soft-polyhedra composed of gels

and polymers of importance in tissue engineering and biomaterials science. I also describe an approach to use polyhedra patterned with circuits and semiconductor chips to create 3D computational devices by aggregation.

In summary, the thesis provides new insight and a robust engineering strategy to mass produce patterned micropolyhedra in a cost-effective manner with material versatility and high yield. In addition to demonstrated applications, we anticipate that these micro polyhedra will offer new capabilities in optics, electronics, robotics, materials science and biomedical engineering.

Advisor: David H. Gracias, Ph.D.

Readers: Howard Katz, Ph.D., Peter Searson, Ph.D., Joelle Frechette, Ph.D.,
Jeffrey Gray, Ph.D.

Acknowledgements

I take this opportunity to express my gratitude to my advisor Prof. David Gracias for giving me an opportunity to work with him. I am very grateful to him for all his help, support and guidance at each and every step. I thank my collaborators Prof. Govind Menon, Prof. Christof Teuscher and Prof. Nick Macias. Thanks to all the past and present lab members I worked with. Thanks to Sachin, Si-Young, Jaehyun, Kate, Teena and Joyce for their help and support. I extend my gratitude to Rohan, Jatinder and Evin for their constant guidance and encouragement. I am very thankful to Pedro, ChangKyu, Hyerin, Qianru, Tao, Zhilin and Jin for all their help and support. Heartfelt best wishes to all of them! I would remain indebted to my family for everything. I acknowledge research funding support from the National Science Foundation.

Table of Contents

List of figures

1. Introduction

Polyhedra are most fundamental shapes widely observed in nature from pollen grains on the millimeter scale to viruses on the nanoscale. Considering structural and functional versatility of natural systems, with the recent developments of engineering and technology one of the important goals has been to develop biologically inspired materials and devices by understanding and mimicking the mechanism of formation of naturally existing systems. In nature, biological molecules such as viruses with polyhedral geometry are formed in a highly parallel assembly process. However, the parallel synthetic fabrication of such precisely patterned three dimensional structures which could provide significant value in biomanufacturing, drug delivery, aggregative self-assembly and the colloidal sciences is challenging. Developing 3D microstructures with high yields using self-assembly techniques wherein physical forces derived from surface tension fold 2D templates into 3D shapes could enable tremendous advancement in various fields in science and engineering, there is a need to uncover underlying geometric design rules that govern the self-assembly processes both in natural self-assembly, such as polyhedral virus assembly and synthetic self-assembly systems such as surface tension driven self-assembly of polyhedra.

1.1 A brief history of polyhedra

Polyhedra have been studied since the days of Plato over 2000 years ago. One of the earliest discussions on polyhedra is found in Plato's dialogues- *Timaeus*, in which he

explained the structure of matter and proposed that the universe is made up of four fundamental elements--fire, earth, air and water and these fundamental elements are solids bounded by plane surface and composed of triangles.[1, 2] Thus, in his discussions, fire, earth, air and water were represented by tetrahedron, cube, octahedron and icosahedron (**Figure 1.1**). The universe made of these four elements was represented by dodecahedron. In addition to describing the structure of matter, Plato also tried to explain the formation of different substances as a result of interaction of these four fundamental elements and how one substance can be transformed into another substance. For example, he explained when water (icosahedron, 20 triangles) is heated by fire (tetrahedron, 4 triangles), the sharp corners of fire (tetrahedron) element break down the water element into their 20 constituent triangles and these triangles recombine to produce 2 air particles (octahedron) and one fire particle (tetrahedron). To arrive at this conclusion, Plato balanced number of constituent triangular faces both the sides as follows:

$$< \text{water} > \longrightarrow 2< \text{air} > + < \text{fire} >$$

< water >		2< air >	+	< fire >
Icosahedron		2x Octahedron		Tetrahedron
20 faces		2x8 faces		4 faces
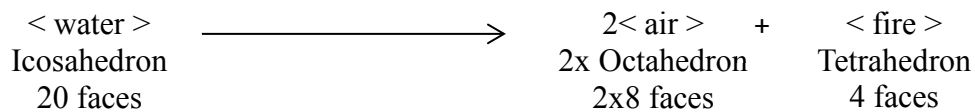
In Plato's description, water represented liquids and air represented gases. It is important to note that Plato's approach of understanding nature by representing fundamental elements with polyhedral shapes and using mathematics to explain phase transformation from liquid to gas has had far-reaching consequences. In fact, with the help of geometry and mathematics Plato sought a kind of 'physical chemistry' to explain how fundamental particles (fire, earth, air and water) interact.[1] The five regular polyhedra-tetrahedron, cube, octahedron, dodecahedron and icosahedron were named as Platonic polyhedra.

1.2 Naturally occurring polyhedra

Polyhedral shapes are widely observed in nature such as organic and inorganic molecules, crystals, pollen grains, honeycomb cells and polyhedral viruses.[3, 4] Several organic and inorganic molecules, such as bucky ball, fullerene chromium hexacarbonyls, transition metal hexafluorides and silicon clusters have predominantly polyhedral geometry.[5-8]

Polyhedral shapes appear in biology as well. An important example of natural polyhedral system is biological self-assembly of bacteriophage viruses such as T4 and MS2. Early crystallographic studies of viruses in the 1940s and 1950s, found that many viruses possess either helical or icosahedral symmetry.[9, 10] A T4 bacteriophage consists of a double stranded DNA genome enclosed in an icosahedral head also known as a capsid, a cylindrical tail sheath, and six legs which are geometrical assemblies of DNA and a hundreds of protein molecules. When T4 infects a bacterium it hijacks the cellular machinery of the host bacterium and utilizes to synthesize copies of these components in large numbers inside the host and then self-assemble to form the final polyhedral structure of the virus. Similarly, the MS2 capsid consists of 180 copies of the coat protein and one unit of the maturation protein which serves as a terminal point. The units of the coat protein are arranged in a manner that has rotational icosahedral symmetry.

1.3 Role of polyhedral shapes in Chemistry

Polyhedral geometries are not new to Chemistry. In fact, Jacobus van't Hoff was the first to suggest that molecules have three dimensional spatial structures assuming that the chemical bonds between carbon atoms and their neighbor atoms were directed toward corners of a regular tetrahedron with the sp^3 carbon atom at the center. He used cardboard models to represent tartaric acid, malic acid, and succinic acid (**Figure 1.2**).[11] Also, the first studies of conformational changes in cyclohexane were illustrated by Hermann Sachse (1890) by folding planar nets into polyhedra.[12] He folded paper models of ideal chair and boat conformations of cyclohexane to demonstrate the fact that allowing carbon atoms to lie outside the plane could alleviate the angle strain in cyclohexane molecules and thus proposed the existence of chair and boat conformations of cyclohexane (**Figure 1.3**). Later Ernst Wilhelm Max Mohr elaborated on the Sachse concept of strainless, 6-membered rings, but made his point more clearly with illustrations of ball-and-stick models (rather than solid tetrahedral).[13] Thus, polyhedral models were the first of the molecular models utilized to study molecular structures although these polyhedral models were not actual visualization of molecular structure rather they were used as didactic tools to explain interatomic bonding and molecular structures.

1.4 Synthetic polyhedra

With growing interest with micro and nanotechnology, researchers have tried to go beyond simple geometries such as cylinders, rods, spheres and have been able to synthesize polyhedral shapes successfully. Such examples include polyhedral shapes made of organic molecules, nucleotides, protein molecules, semiconductors, polymers and metals. These polyhedral shapes have been used for biotechnology, electronics, drug delivery, chemical reaction diffusion systems and shown that polyhedral shapes have certain advantages, such as anisotropy, surface interaction, precise patterning, over spherical shapes where sphere do not exhibit these properties.

1.4.1 Polyhedral hydrocarbons

Polyhedral hydrocarbons are synthetic organic molecules that have the shapes of platonic solid geometries with carbon atoms as the vertices and chemical bonds as the edges. Polyhedral hydrocarbons have been synthesized in both Platonic and Archimedian shapes.

Among Platonic polyhedral hydrocarbons, synthesis of only cubane, and dodecahedrane has been reported (**Figure 1.4**).[14-16] The fact that a carbon atom is tetravalent, the synthesis of icosahedrane is not possible because in icosahedron each vertex is bonded with five edges. Similarly, since dihedral angle in octahedral shape is 109.5^0 which is same as the bond angle for *sp³* carbon atoms, it is not likely for a hydrocarbon to exist as the

octahedrane. In an octahedron, there are 6 vertices that are connected to 4 edges each. In case of octahedrane there would be no hydrogen atoms and the valency of each carbon atom will be satisfied through c-c bondings. Thus this hypothetical octahedral molecule would not be a hydrocarbon but just an allotrope of elemental carbon C_6. Existence of octhaedrane cannot be ruled out completely but theoretical modeling suggests it is very unlikely. However, both octahedral and icosahedral compounds have been observed for boron compounds.[17]

Although tetrahedrane derivatives have been synthezied but the synthesis of tetrahedrane has not been reported yet but the calculations show it will be kinetically stable in spite of the acute bond angle and consequent angle strain.[18] As the number of carbon atoms increases the polyhedral geometry more closely approximates to a sphere. Bucyballs or spherical fullerene consists of 60 carbon atoms (C_{60}) and has a shape of truncated icosahedron, an Archimedian polyhedron.

1.4.2 Biomolecular polyhedra

DNA hybridization offers assembly of nucleotides due to base pairing into complex polyhedral structure in a high through put programmable and precise manner. Multiple DNA strands with complimentary sequences are when annealed in presence of polymerase enzymes, double stranded architectures are formed. In terms of achieving a rational design and predictability of the final 3D architecture, *in silico* approaches can easily be used to design nucleotide sequence in such a way that final desired 3D architectures are formed.

In 1991 Nadrian Seeman synthesized a cube made up of single stranded DNA molecules, the first synthetic three-dimensional nucleic acid nanostructure.[19] This followed synthesis of other complex polyhedral structures such as truncated octahedron, and icosahedron.[20, 21] But it was soon realized that these polyhedral structures were not rigid enough to sustain shapes of more complex higher order polyhedral shapes. In order to increase rigidity of DNA structures, Paul Rothemund utilized DNA origami approach to form programmable DNA structures. The technique involves hybridization of long DNA strands and shorter segments where longer strands form scaffold and shorter segment help them fold at specific positions. Using origami approach, synthesis of a DNA cube with controllable lid was successfully demonstrated (**Figure 1.5**).[22]

1.4.3 Nano and microscale polyhedral shapes by surface forces

Surface tension and intrinsic stress driven self-assembly technique offers an approach to fabricate polyhedral structures at nanoscale. In this approach, 2D nets of a desired polyhedron are lithographically defined on a silicon substrate and developed with thermal evaporation or sputtering of metals or dielectrics such as nickel and alumina, the hinge gaps are made of tin. When these 2D nets are subjected to reactive ion etching, underlying silicon layers is etched off, thus heat generated melts Sn and causes self-folding into nanoscale shapes.
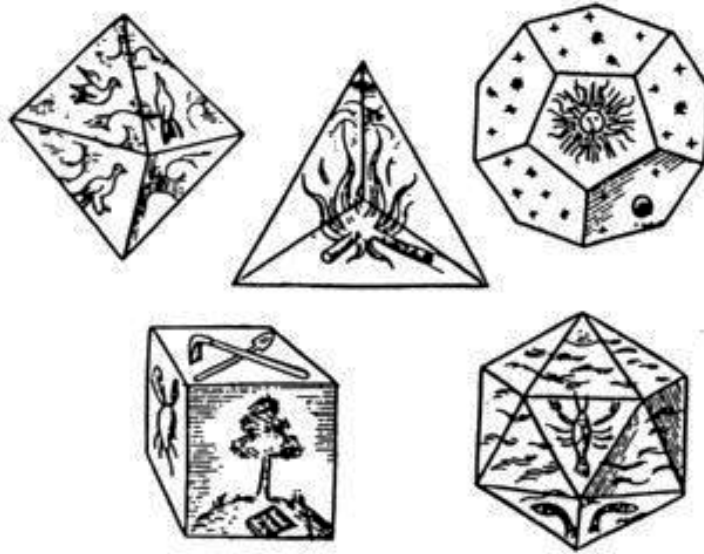
Figure 1.1 Platonic polyhedra representing fire (tetrahedron), earth (cube), air (octahedron), water (icosahedron) and the universe (dodecahedron). Printed with permission from Ref[1] © Cambridge University Press, 1997.

Figure 1.2 van't Hoff polyhedral models of organic molecules. Reprinted with permission from Ref[11] Photo: Deutsches Museum.
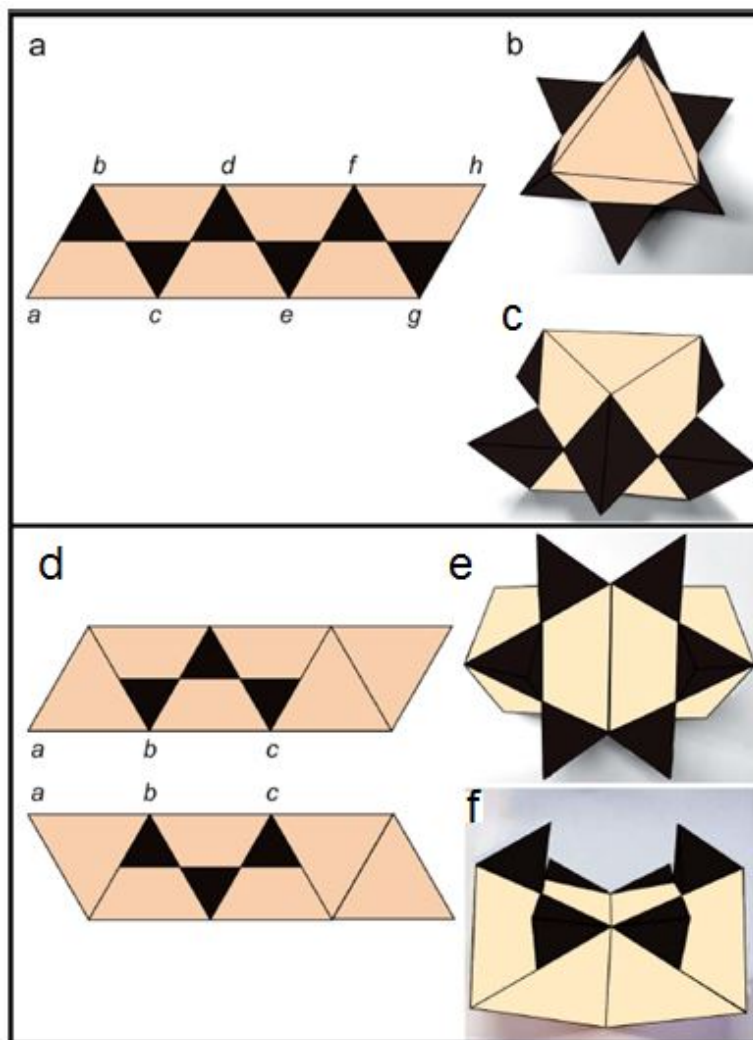
Figure 1.3 Sachse's polyhedral model of cyclohexane. (a) shows the 2D net that generates chair conformation of cyclohexane when folded along the edges *bc, cd, de, ef, fg* and the edges *ab* and *gh* are glued together; and van't Hoff tetrahedra are attached on the dark triangles. The center of each van't Hoff tetrahedron represents carbon atom. (b) top and (c) side views of Sachse's paper model of chair form of cyclohexane; (d) the two nets shown are when folded along the edges and the vertices a, b, c are glued together and van't Hoff tetrahedron is attached on each dark triangle, generate boat form of cyclohexane. (e) and (f) are top and side views of Sachse's paper model of boat conformation of cyclohexane.
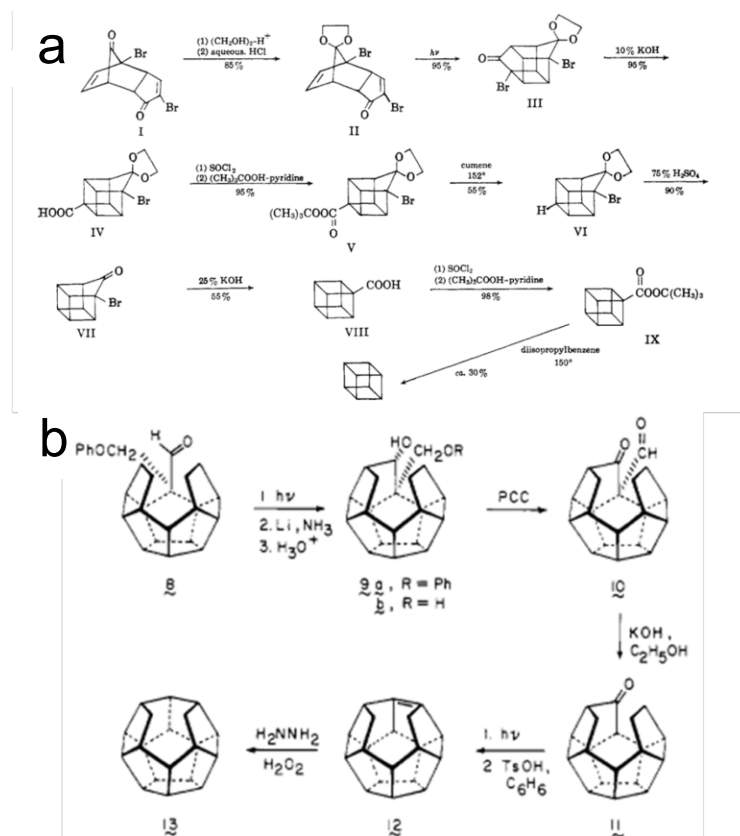
Figure 1.4 Synthesis of Platonic hydrocarbons (a) synthesis scheme of cubane. Reprinted with permission from Ref[14] © American Chemical Society, 1982. (b) synthesis scheme of dodecaehdrane. Reprinted with permission from Ref[16] ©American Chemical Society, 1982.
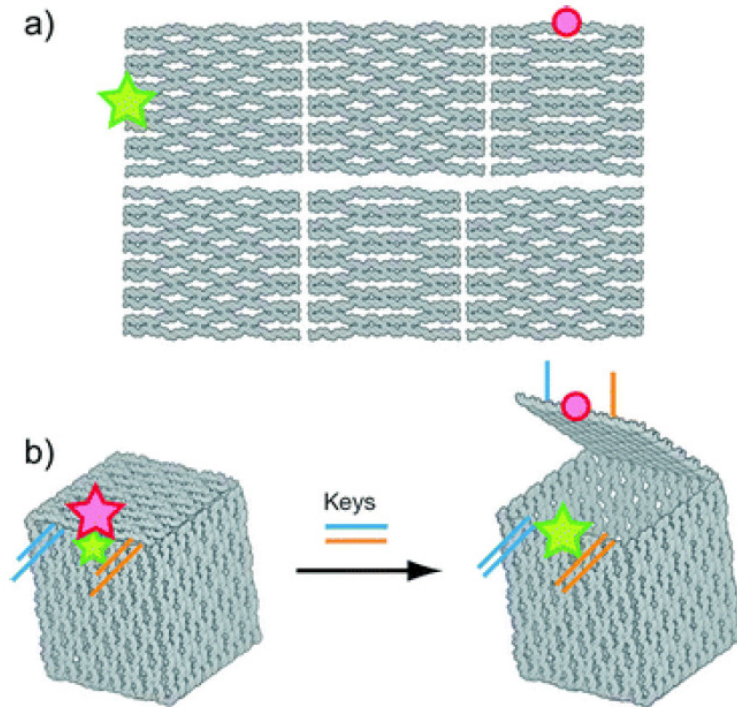
Figure 1.5 Three dimensional DNA polyhedron (a) Nucleotide template and (b) 3dimensional lid controlled cubic structure. Reprinted with permission from Ref[22] © Mcmillan Publishers Ltd (Nature Publishing Group), 2009.

2. Thesis overview

The body of work presented in this thesis is focused on following:

1. **Uncovering geometric design rules of self-assembly with theory and experiments:** Model polyhedral systems dodecahedra, truncated octahedra and icosahedra have been utilized for understanding self-assembly process in a synthetic system and underlying geometric rules have been investigated. Findings reported have been contrasted with biomolecular self-assembly systems such as protein folding and virus capsid assembly.

2. **Formation of structural isomers in a synthetic self-assembly:** A mesoscale polyhedral model has been investigated for the formation of octahedral isomers. In this part of work, the roles of assembly pathways and degrees of freedom of intermediates have been studied to show how the formation of one isomer over the other can be enriched by engineering assembly pathways via manipulation of degrees of freedom of initial precursors. Also, the findings have been contrasted with polyhedral models of chair and boat conformations of cyclohexane.

3. **Fabrication of soft polyhedra by folding and molding:** In this part of thesis a process combining surface tension driven self-assembly and molding methods to create micropolyhedral structures with precise surface morphologies has been

discussed. A method to create cell-laden bio-blocks and its potential application in tissue engineering has been discussed. Also, it has been shown how mechanical strength of building blocks can be controlled via engineering shapes of building blocks.

4. **Three dimensional computational devices using polyhedral electronic blocks (E-blocks):** In this part of the thesis, an approach for building three dimensional computer architecture using polyhedral E-blocks has been discussed. The approach presents an approach of utilizing the third dimensions for integration of electronic elements such by self-assembly techniques.

3. Surface tension driven self-assembly of micropolyhedra[*]

There are numerous techniques such as photolithography, electron-beam lithography and soft-lithography that can be used to precisely pattern two dimensional (2D) structures. These technologies are mature, offer high precision and many of them can be implemented in a high-throughput manner but the advantages of planar lithography can be leveraged and combined with self-folding methods[23-31] wherein physical forces derived from surface tension are used to curve or fold planar structures into three dimensional (3D) structures. In doing so, it is possible to mass produce precisely patterned static and reconfigurable particles that are challenging to synthesize.

In this chapter method to create patterned micropolyhedra, notably, permanently bonded, hollow, polyhedra that self-assemble and self-seal due to the minimization of surface energy of liquefied hinges[32-34] has been detailed. These methods can be used to create micropolyhedra with overall sizes ranging from the micrometer to the centimeter length scales. Further, arbitrary patterns can be defined on the surfaces of the polyhedra of importance in colloidal science, electronics, optics and medicine. More generally, the concept of self-assembling mechanically rigid polyhedra with self-sealing hinges is applicable, with some process modifications, to the creation of polyhedral structures at even smaller, 100 nm length scales[33, 35] and with a range of materials including metals[32], semiconductors[28] and polymers[36].

---

[*]Parts of this chapter have been adapted from Pandey S., Gultepe E. and Gracias D.H. "Origami inspired self-assembly of patterned and reconfigurable particles" *J. Vis. Exp.* 72, e50022 (2013).

3.1 Fabrication details

For surface tension driven assembly, the polyhedra can be fabricated in a high throughput manner in which prepatterned 2D nets of a desired shape self-fold and self-seal into closed polyhedra due to minimization of surface energy of the molten hinges.[36, 37] First, at least two mask sets are needed, one for regions that do not bend or curve (rigid panels) and the other for regions that bend, curve or seal (hinges). Additional masks can be utilized to define surface patterns of pores, molecular patches, optical or electronic elements. Masks are designed using a variety of two dimensional vector graphics software programs such as AutoCAD, L-Edit or Adobe Illustrator and then printed on transparency film to make photomasks. Using these photomasks lithography, electroplating and wet etching techniques are utilized to pattern 2D panels and solder hinges. The materials for the panels and hinges should be chosen so that the hinge material has a lower melting point than the panels and hence the panels remain rigid while the hinges are melted. Assembly occurs when the templates (hinges panels) are released from the substrate by dissolving sacrificial layer and heated above the melting point of the hinge material. For example, in case of metallic particles with Ni panels, Pb-Sn solder is deposited on the hinges which melts at ~200 °C and prompts the folding. Similarly, in the case of polymeric particles with SU8 panels, polycaprolactone hinges can be deposited which assemble at ~58 °C on heating in water. [31, 34-37] The process works best when the hinge material is pinned within the hinge region during reflow; *i.e.* it does not spread all over the panels and does not completely dewet from the panel. This pinning can be achieved by the selection of materials with appropriate wetting characteristics and viscosity. A schematic illustration of self-folding process is shown in **Figure 3.1.**

3.2 Design rules

Empirical studies suggest the following optimal design rules for generating masks that can be used for the surface tension driven folding of a polyhedron of side length L.(1) For a particular polyhedral geometry, the number of panels first needs to be determined. For example, a cube has six square panels while a dodecahedron has twelve pentagonal panels. (2) The high-yielding two dimensional arrangement of panels, also called a net needs to be figured out. (3) In the panel mask, the panels of the polyhedra should be drawn as nets and the adjacent panels should be spaced by a gap of width that is approximately 0.1L. Registry marks are needed for subsequent alignment with the hinge mask.

In the hinge mask, both folding hinges (in between the panels) and locking or sealing hinges (at the edges of the panels) must be defined. Folding hinges should have lengths of 0.8L and widths of 0.2L while sealing hinges at the periphery of the panels should have lengths of 0.8L and widths of 0.1L with an overhang of 0.05L **(Figure 3.2)**. Special care must be taken to ensure that the panel and hinge masks overlay, with registry. With this design rule, we have been able to synthesize particles with sizes ranging from 15 μm to 2.5 cm.

The volume of the hinge controls the folding angles, and for a given hinge width, finite element modeling is required to determine the necessary thickness of the hinge.[37-40] (**Figure 3.3**). However, the attractive feature of this approach is the use of locking or sealing hinges which provide considerable error-tolerance during self-assembly process. Hence, when sealing hinges are used, the assembly process is tolerant to deviations in hinge volumes, allowing

them to be only approximately targeted. Due to significant cooperativity during self-assembly, complex shape polyhedra such as dodecahedra or truncated octahedral can be mass produced.

3.3 Mechanism of surface tension driven self-assembly

In the self-assembly experiments reported in thesis the size of polyhedral range from 300 μm to 2 mm; the hinges are made of Sn-Pb solder. In order to understand the mechanism surface tension driven assembly, it is important to contrast the relative magnitude of capillarity and thermal fluctuations. For a polyhedron with side length of 300μm, the sides of hinges are in the range 30μm–60μm, so the area of the solder is on the order of $10^{-8}m^2$. A typical value of the surface tension of solder is 0.5N/m. Thus, an approximate scale of the capillarity is 10^{-8}J. The temperature of the solvent is ~ 200°C = 473K, which gives typical thermal energy kT = 6.5×10^{-21}J. Thus, capillarity strongly outweighs thermal fluctuations.

In order to model the hinge, the dynamics, gravity and three dimensional effects can be neglected. In static equilibrium, the Young-Laplace law tells that the interface of the solder droplet is a circular arc that meets the panel at the wetting angle. The experimental setup determines the area of the solder droplet and the wetting angle. These two variables then determine the angle of hinge rotation. There are three cases, as shown in **Figure 3.4**. The crucial assumption is that molten solder does not wet the adjacent parts of the panels thus remains pinned in the hinge area on melting. This implies $\frac{\pi}{2} < \beta < \pi$. Let L denote the length of the segments AP and BP. With some basic trigonometry the area of the droplet $A(\emptyset)$ can be calculated as:

18

$$R = L\frac{\cos\phi}{\sin(\beta-\phi)}, \quad A(\phi) = R^2(\beta-\phi) - LR\cos\beta, \quad \pi/2 < \beta < \pi.$$

In this regime, the area strictly decreases with $\emptyset$ and can be inverted to yield $\emptyset(\beta, A)$. Thus, the amount of solder deposited controls the angle of rotation of the hinge. When the droplet wets the panel $\beta \in \left(0, \frac{\pi}{2}\right)$, the area is not a monotonically decreasing function of A when the droplet wets the panel $\beta \in (0, \pi)$ and there can be two positions of static equilibrium for a given area. To summarize, it is necessary that the panels are not wet by the solder. A schematic of surface tension driven folding is shown in **Figure 3.5**.

3.4 Versatility of the self-assembly process

The origami-inspired surface tension driven self-assembly process is versatile and can be used for synthesizing a variety of 3D static and reconfigurable particles with a wide range of materials, shapes and sizes (**Figure 3.6**). Further, the ability to precisely pattern sensors and electronic modules on these particles is important for optics and electronics. In contrast to patchy particles formed by alternate methods, where patterns are relatively imprecise, this methodology provides a means to synthesize precisely patterned particles. In surface tension based assembly, the use of liquefying sealing hinges ensures that the particles are well sealed and mechanically rigid after assembly (on cooling). Previously, we have observed that the seams are leakproof even for small molecules[41, 42]

3.5 Conclusions

In summary, the surface tension driven self-assembly process is highly parallel and 3D structures can be fabricated and triggered simultaneously. Additionally, precise patterns as exemplified by square or triangular pores can be defined in all three dimensions, and on selected faces if needed.

a) Clean Si wafer

b) Spin coat PMMA sacrificial layer

c) Evaporate Cr adhesion promoter

d) Evaporate Cu seed layer

e) Pattern panels

f) Pattern hinges

g) Dissolve Cu / Cr layers

h) Release 2D template by dissolving sacrificial layer

i) Heat to self-assemble

j) Rinse self-assembled cube
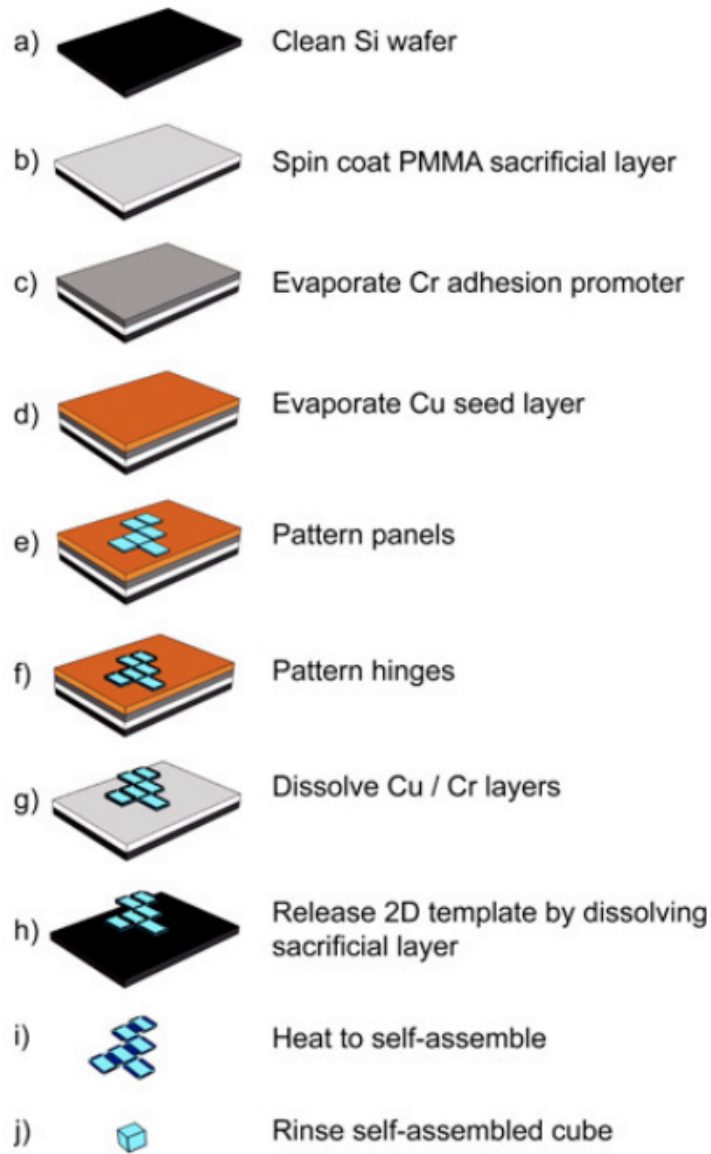
Figure 3.1 Schematic illustration of the important fabrication steps for the surface tension driven assembly a cube shaped polyhedron.
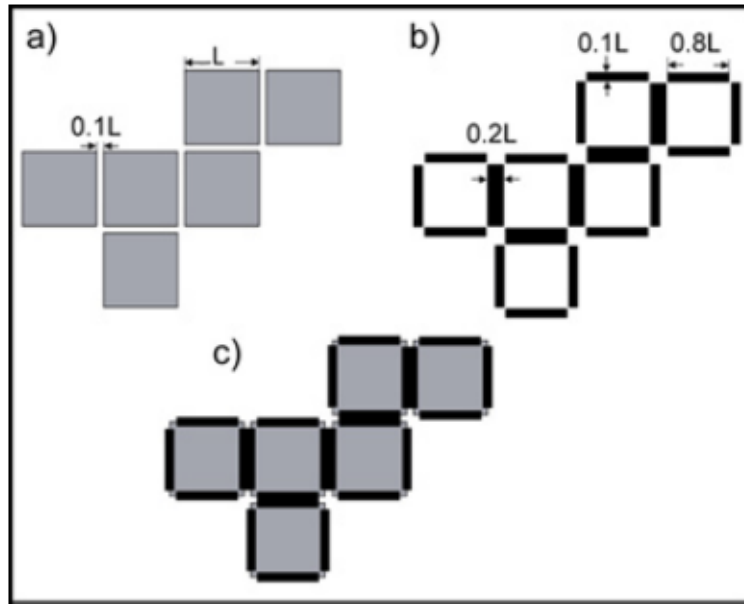
Figure 3.2. Mask design rules for self-assembled micropolyhedra: (a) Schematic of the panel mask for a polyhedron of side length L, (b) schematic of the hinge mask featuring folding (0.2 L x 0.8 L) and locking or sealing (0.1 L x 0.8 L) hinges, and (c) schematic of the overlaid 2D precursor or net showing hinges panels.
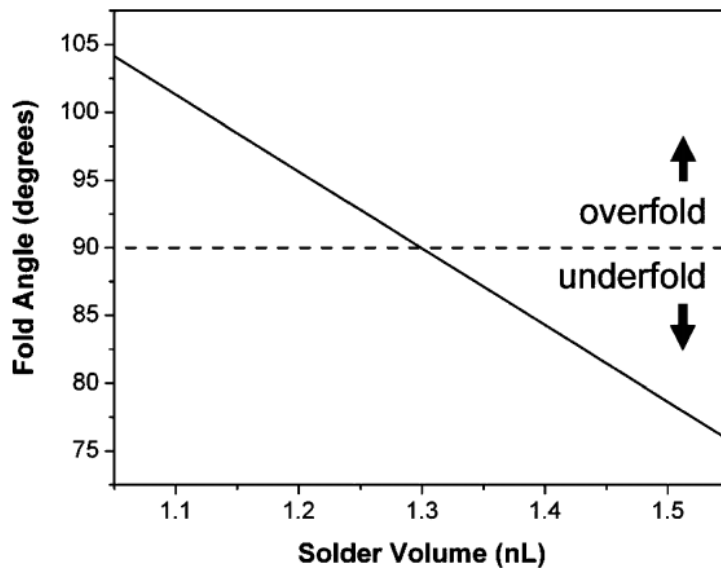
Figure 3.3 Simulation results showing the dependence of fold angle on solder volume for self-assembly of a 200 µm size cube. Reprinted with permission from Ref.[37] © 2007, American Chemical Society
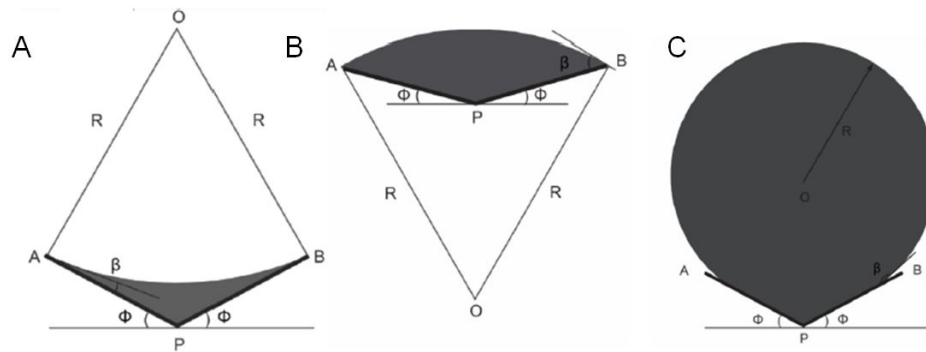
Figure 3.4 Mechanism of surface tension driven self-assembly. Shaded area represents molten solder droplet, β is the wetting angle and $2\emptyset$ is the angle of rotation of the hinge. (a) Wetting and a concave interface, $0 < \beta < \emptyset$; (b) Wetting and a convex interface $\emptyset < \beta < \pi/2$; (c) Non-wetting and a convex interface, $\frac{\pi}{2} < \beta < \pi$.
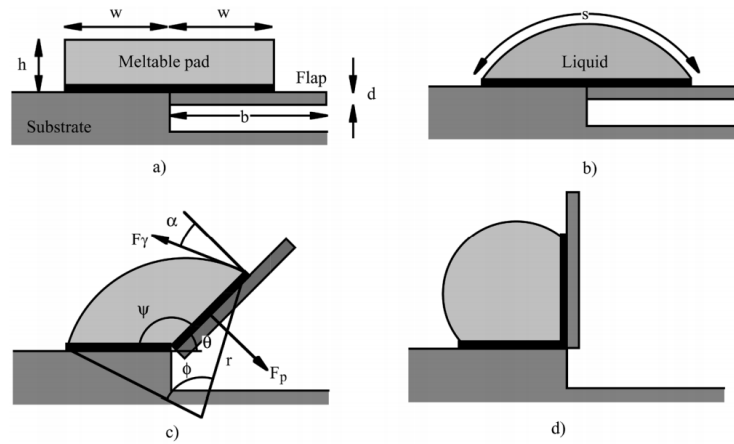
Figure 3.5 Surface tension powered rotation of panels. When the meltable pad melts, the panel rotates to the equilibrium condition. Reprinted with permission from Ref.[29] © 2003, IEEE.
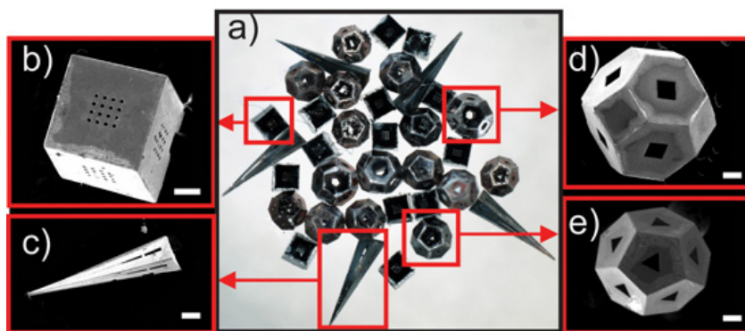
Figure 3.6 Images of origami inspired self-assembled patterned micropolyhedra. (a) Optical image of self-assembled particles in a variety of shapes. (b-e) SEM images of a (b) self-assembled porous cube, (c) pyramid, (d) truncated octahedron and (e) dodecahedron.

4. The role of compactness for polyhedral self-assembly[*]

Self-assembly has emerged as a paradigm for highly parallel fabrication of complex three-dimensional structures. However, there are few principles that guide *a priori* design, yield, and defect tolerance of self-assembling structures. In this chapter, self-assembly experiments and theory of the geometric principles that underlie self-assembly of polyhedra from two-dimensional nets have been detailed. For any given polyhedron, polygonal panels can be arranged in many ways thus there is a large number of nets that can be used for self-assembly of polyhedral from 2D nets; e.g. the six panels of a cube can be arranged in eleven ways that fold into a cube, thus the cube has 11 nets. Similarly the dodecahedron and icosahedron have 43,380 nets each, and 14 faced truncated octahedron has 2.3 million nets of which only some are favor a high yield of self-folded structures. As the number of panels increase, there is a combinatorial explosion for the number of nets. Hence there was a need to develop a net search algorithmic approach that could be used to find best nets based on arrangement of panels on 2D, which consequently result into high yield. With experiments and theory the geometric principles that govern self-assembly of polyhedra from two-dimensional nets were examined. In particular, an algorithm to find the optimum nets for self-folding of a given polyhedron was developed and then validated experimentally. The findings reported in this chapter reveal design rules based on geometric considerations similar to hydrophobic zipper hypothesis in protein folding; and the stabilizing role of distinguished intermediates in folding pathways as in the assembly of viral capsids.

---

[*] Parts of this chapter have been adapted from Pandey S., Ewing M., Kunas A., Nguyen N., Gracias D.H. and Menon G. "Algorithmic design of self-folding polyhedra", *Proc. Nat. Acad. Sci*, 108 (50), 19885-19890 (2011).

4.1 Motivation from biomolecular assembly

Nature uses hierarchical assembly to construct essential biomolecules such as proteins and nucleic acids and biological containers such as viral capsids. Increased understanding of biological systems has inspired several synthetic methods of self-assembly.[43] Conversely, part of the promise of synthetic self-assembly has been that it may yield essential insights into the formation of biological structure. In order to realize these ambitions, it is necessary to develop model experimental systems and theoretical analyses that make precise the analogies between natural and synthetic self-assembly. Abstraction of the essentials of complex biochemical processes is an important step in this process, and perhaps the simplest abstraction is of the geometric form of a biological structure. Two such abstractions are the Caspar– Klug (CK) theory of viral structure and hydrophobic-polar (HP) lattice models for protein folding.[44, 45] The consequences of geometry alone can be striking in such models: The CK theory provides a valuable classification of virus shapes by T number, and much of the detailed architecture of compact proteins such as helices, and antiparallel and parallel sheets emerges from purely steric restrictions on long chain molecules.[46, 47] Building such geometric models is, of course, part of a long tradition in biochemistry. What is now striking is the ability to build basic geometric structures such as polyhedra in laboratory self-assembly experiments using molecules such as DNA or 100-nm to 1-mm scale lithographically interconnected panels.[37, 48-51] A comparison of self-assembly models such as protein folding, viral capsid assembly is shown in **Figure 4.1**.

4.2 Geometric considerations for the algorithmic design

Nets have traditionally been used to build models of polyhedra from a stiff material such as cardboard. They first appear explicitly in Dürer's work in the 15th century and have been used to build a complete set of Archimedean and Platonic solids.[52] It is not known if every convex polyhedron has a net nor are there systematic estimates of the number of nets for a given polyhedron, though the number is known for Platonic solids.[53, 54] As mentioned earlier tetrahedron has two nets, the cube and octahedron have 11 nets each, and the dodecahedron and icosahedron have 43,380 nets each. Interestingly the truncated octahedron has approximately 2.3 million nets. Such a combinatorial explosion creates an interesting conundrum for engineering design: What criteria determine self-folding with high yield? How to search efficiently for the "best" net within such a large set? In order to consider geometric design rules based on arrangement of panels in 2D, it is important to consider both metric and topological measures.

4.2.1 Radius of gyration and vertex connections as design criteria

Since the nets for a given polyhedron differ in their geometry and combinatorial topology, both metric (radius of gyration) and topological (number of vertex connections) measures were used in self-assembly studies. These two measures ensure the compactness of nets. In case of protein folding due to hydrophobic-hydrophobic interactions, two hydrophobic groups that interact are the topological neighbors. Taking the analogy from protein folding where most compact amino acid chains fold faster, it was

hypothesized that that the most compact 2D nets should give the best yield on self-assembly. Thus both the *Rg* and *Vc* were considered for compactness of a net.

Radius of gyration *Rg* of 2D net is defined as:

$$(\bar{x}, \bar{y}) = \int_{\Omega} (x,y) dA, \qquad R_g^2 = \int_{\Omega} (x - \bar{x})^2 + (y - \bar{y})^2 dA.$$

Lower value of *Rg* insures that the panels are not "too spread" in 2D space and thus are compact. This compactness criterion based on *Rg* is metric.

Similarly a topological measure, the number of vertex connections (V_c) was defined as, a vertex connection is a vertex that is shared by two panels that do not share any edges. The dodecahedron net shown in **Figure 4.2** has 10 vertex connections. It is important to note that both *Rg* and *Vc* are measures of compactness but both are distinct. Considering these two parameters the self-assembly experiments were performed.

4.3 Experimental details

All 43,380 nets for the dodecahedron and icosahedron, and 123,452 nets (of 2.3 million estimated nets) for the truncated octahedron were tabulated using a Monte Carlo scheme. From these nets three nets for each polyhedron: the most compact, the least compact, and the median for each of the two compactness criterion were chose for self-assembly experiments. Several nets may have the same *Vc*, so when choosing nets according to *Vc* the following choices were made: Among all maximum *Vc* nets, choose the net with smallest *Rg*

; among all minimum Vc nets, choose the net with highest Rg; and among all nets with the median Vc, choose the net with median Rg. Fifty samples of each of these nets were self-assembled experimentally with the self-assembly methods detailed in chapter 3.

Briefly, Autodesk AutoCAD was used to draw nets and then printed on transparency sheets to make photomasks. Sides of a panel measured 300 μm, with two adjacent panels spaced apart by a width equal to 10% of the panel edge length. Optical lithography was used to develop features on a silicon wafer, and nickel and solder were electrodeposited on the panels and hinges, respectively. All Vc and Rg nets for a polyhedron were processed across the same wafer with a uniform random distribution of nets to minimize processing variations during lithography, electroplating and etching. The nets were released from the substrate with nickel panels connected with Sn-Pb solder hinges and the free-standing structures were heated in a high boiling point organic solvent until they assembled. All the nets for fixed polyhedra were self-assembled in close proximity in a petri dish in order to minimize the effect of variation in temperature and fluidic agitation. After self-folding, the solution was allowed to cool down gradually. The molten solder solidified on cooling and the polyhedra were held robustly in place. Self-assembled 3D structures realized from each net were carefully examined under an optical microscope and graded into three categories—A, B, and C. Grade-A polyhedra had no discernible defects when examined under an optical microscope. Grade-B polyhedra had the desired shapes but had panels that were misaligned with an angle of 20° or less. Samples with defects more severe than 20° misalignment and with multiple defects were graded as grade-C polyhedra.

4.4 Results and discussion

It was observed that both measures of compactness determine yield for these higher order polyhedral (dodecahedra and truncated octahedra) just as for the cube and octahedron. However, it was found that of the two measures, Vc is a better predictor than Rg. For the dodecahedron, the percentage of A-grade self-assembled polyhedra from nets with the maximum Vc is more than five times than that from nets with the lowest Rg, $Rg = 693.7$ μm. In addition, almost 80% of the maximum Vc samples are of grade A and B as compared with about 20% for the minimum Rg samples. For the truncated octahedron, the percentage of grade-A self-folded polyhedra from nets with the maximum Vc net is two times that of A-grade samples for minimum Rg, $Rg = 795$ μm. Moreover, almost 60% of the maximum Vc samples are of grade A and B as compared with about 30% for the minimum Rg samples. In contrast with these polyhedra, icosahedra could not be assembled from 2D nets. But it is still the case that the more compact nets are less malformed than the others. The representative polyhedral and their yields are shown in **Figure 4.3** and **Figure 4.4**. In further experiments with self-assembly of dodecaehdra and truncated octahedral with same Vc and varying Rg, and it was found that the nets with highest Vc and lowest Rg result the best yields thus confirm that the Vc is a better predictor than Rg (**Figure 4.5** and **4.6**).

The computation of self-assembly pathways of the cube reveals that the self-assembly pathways funnel through some dominant intermediates. As shown in **Figure 4.7** the states 1 and 5 are the most preferred intermediates. The properties of intermediates for higher order complex polyhedra such as octaehdra and dodecahedra are investigated in following chapters.

4.3 Conclusions

The goal of research work detailed in this chapter was to elucidate the geometric principles that underlie self-assembly of polyhedron from 2D nets. It was verified that compactness is an effective design criterion for several polyhedra by computationally exploring a large set of possible nets and testing selected nets experimentally. Also, a discrete configuration space of folding was introduced and found that the geodesic between the 2D net and 3D polyhedron is a useful idealization of experimentally observed pathways of self-assembly of cubes. These findings suggest further studies of self-assembly in order to build more complex shapes and to minimize errors through the loss of rigidity. Although the number of nets is large for the polyhedra that were considered this study, it was still amenable to an exhaustive search, which ceases to be the case for more complex polyhedra such as models for viral capsids. In seeking nets for realistic virus shapes, there are polyhedra with approximately 10^{30} spanning trees (a number obtained from Kirchhoff's matrix tree theorem). It is impossible to find an optimal net and geodesics by an exhaustive search for such polyhedra, and suitable randomized algorithms must be used instead. On the experimental side, the ability to observe pathways provides additional insight into self-assembly. In summary, the main findings reported in this chapter are, (1) compactness is a simple and effective design principle for maximizing the yield of self-folding polyhedra; and (2) shortest paths from 2D nets to 3D polyhedra in the configuration space are important for rationalizing experimentally observed folding pathways and (3) self-assembly pathways funnel through some preferred intermediates.
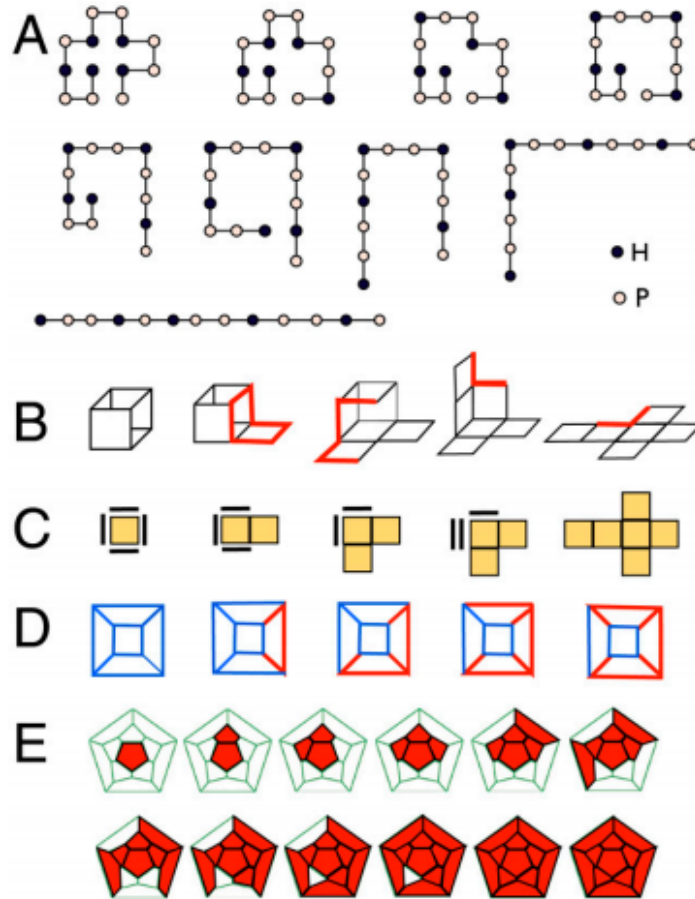
Figure 4.1 Comparison of the discrete geometry of three self-assembly models. (a) Unfolding an HP chain. A compact HP chain on a 2D lattice is unfolded by breaking secondary HH bonds between topological neighbors. At each step, secondary bonds break and/or the chain reduces its discrete curvature. The compact configuration is chosen from ref. 31. The motion of the chain through kink jumps and rigid rotations is adapted from ref. 32. (b–d) Several representations of unfolding a cube. At each step, all edges linked at a vertex connection are cut so that a face is free to rotate rigidly through the dihedral angle, which gives faces linked through vertices but not edges (topological neighbors). (b) A perspective view. (c) A convenient schematic for the plan view. (d) Unfolding as two-color evolution on the graph of the cube: Cut edges are red and constitute a tree that grows at each step. Unfolding is complete when the tree is spanning. (e) Viral capsid assembly. Intermediate stages in the formation of a dodecahedral viral capsid following refs. 30 and 33. At each stage, a new face is added and congruent arrangements correspond to the same intermediate.
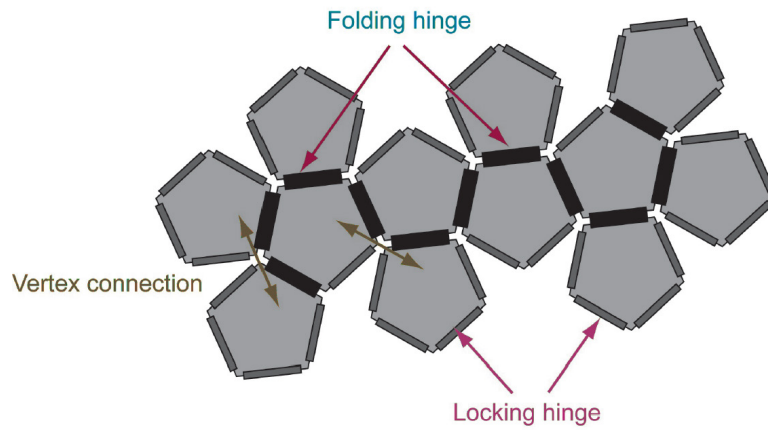
Figure 4.2 A schematic illustration of a dodecahedron net showing panels, internal (folding) hinges, external (locking or sealing) hinges and vertex connections. The net shown has $Vc = 10$.
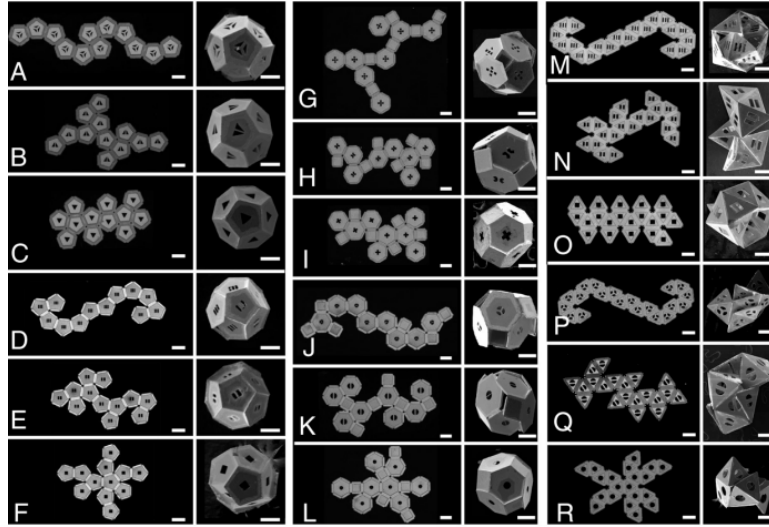
Figure 4.3 Self-folding experiments on nets with varying *Vc* and *Rg*. Optical and SEM images showing photolithographically fabricated panels connected by solder hinges and the corresponding self-folded 3D structures respectively. (A–F) Dodecahedra in the order *Vc* =2, 6, and 10, and *Rg* = 1102.2, 800.9, and 693.7 μm, respectively. (G–L) Truncated octahedra in the order *Vc* = 2, 7, and 12, and *Rg* = 1306.3, 912.7, and 795.0 μm, respectively. (M–R) Icosahedra in the order *Vc* = 26, 38, and 50, and *Rg* = 711.1, 514.6, and 445.4 μm, respectively. (Scale bar: 300 μm.)
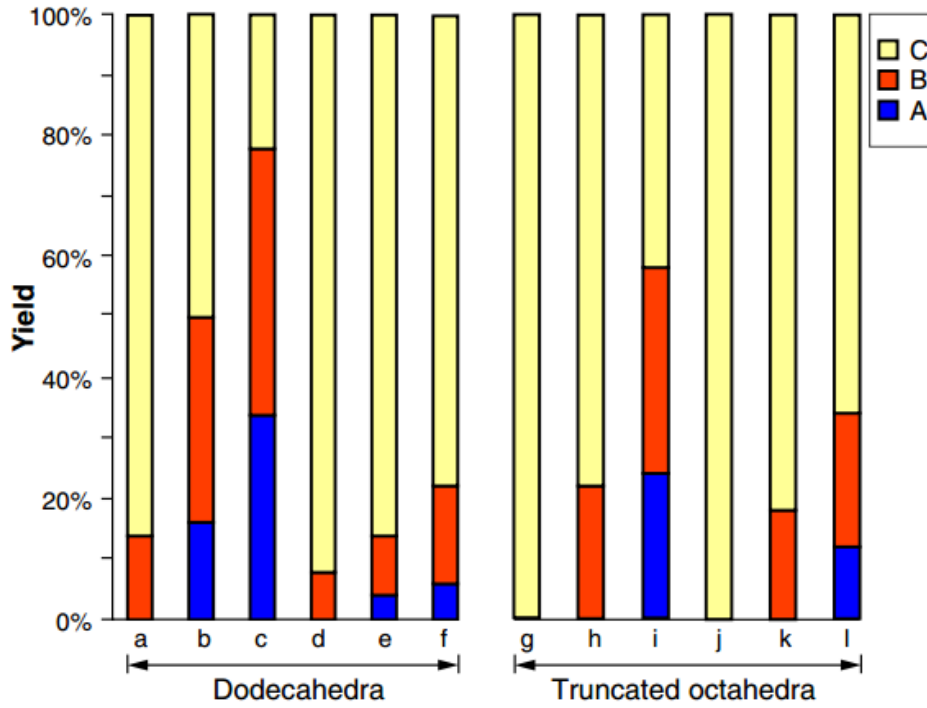
Figure 4.4 Yield measured in self-folding experiments on nets with varying Vc and Rg. (A–F) Dodecahedral nets in the order Vc = 2, 6, and 10, and Rg = 1102.2, 800.9, and 693.7 μm, respectively. (G–L) Truncated octahedral nets in the order Vc = 2, 7, and 12, and Rg = 1306.3, 912.7, and 795.0 μm, respectively.
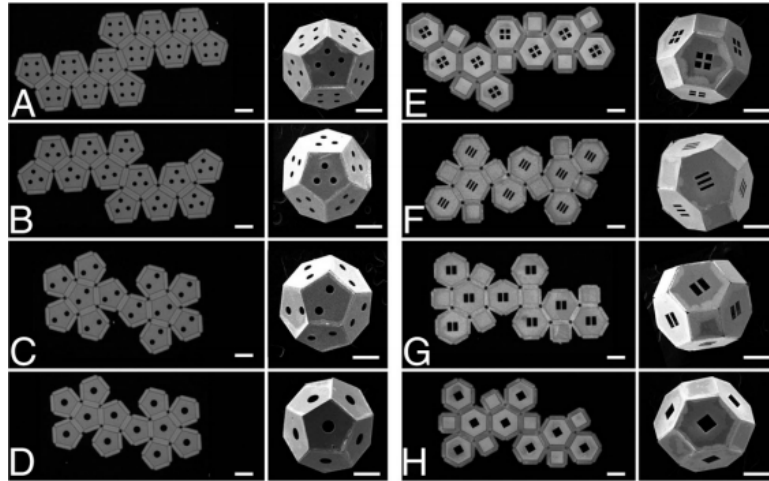
Figure 4.5 Self-folding experiments on high Vc nets with varying Rg. Optical and SEM images. (A–D) Dodecahedral nets with $Vc = 10$ and $Rg = 810.2$, 797.4, 755.4, and 747.7 μm, respectively. (E–H) Truncated octahedral nets with $Vc = 12$ and $Rg = 911.6$, 870.2, 867.4, and 852.8 μm, respectively. (Scale bar: 300 μm.)
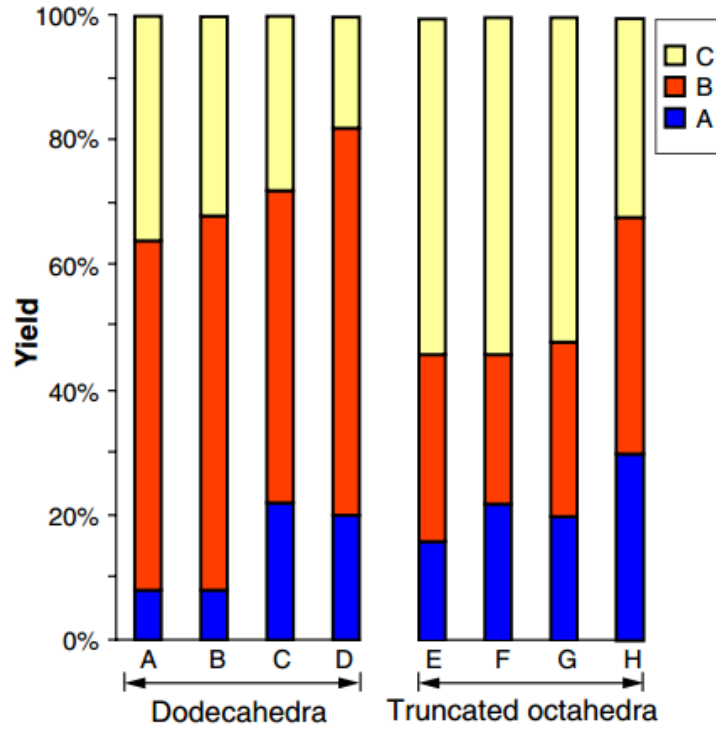
Figure 4.6 Self-folding experiments on high *Vc* nets with varying Rg. Optical and SEM images. (A–D) Dodecahedral nets with *Vc* = 10 and *Rg* = 810.2, 797.4, 755.4, and 747.7 μm, respectively. (E–H) Truncated octahedral nets with *Vc* = 12 and *Rg* = 911.6, 870.2, 867.4, and 852.8 μm, respectively. (Scale bar: 300 μm.)
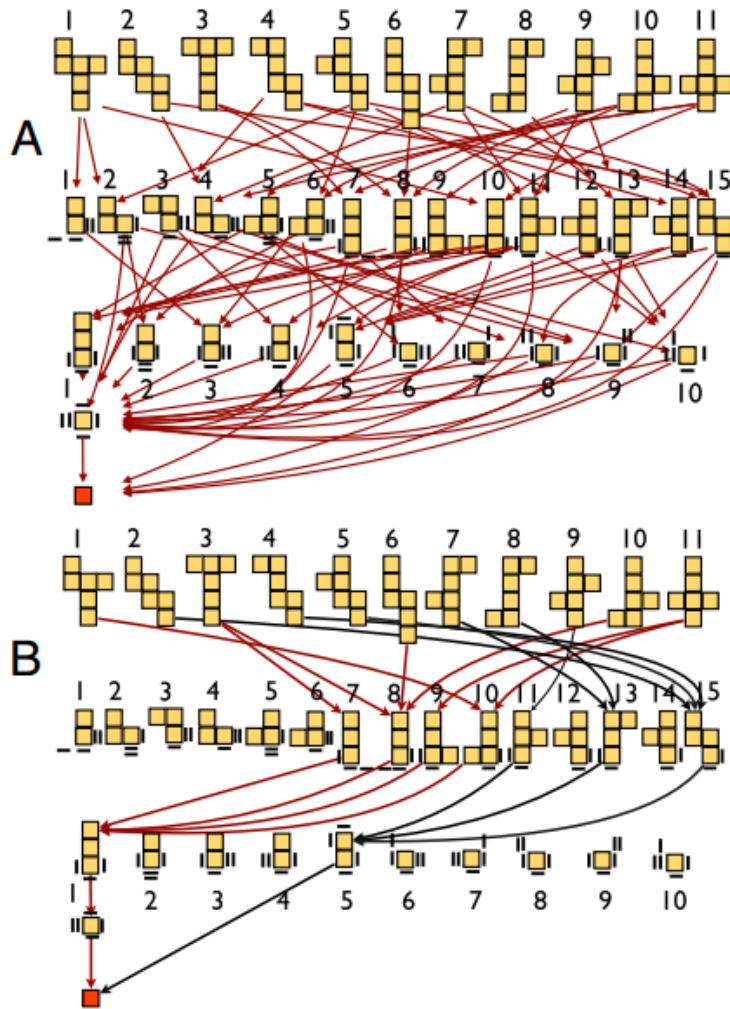
Figure 4.7 (A) Computed configuration space and folding pathways for the cube. Partially folded intermediates and all folding pathways for the cube computed by the gluing at vertex connections algorithm. Multiplicity of edges connecting intermediates is not shown. Double bars denote vertically stacked faces. (B) Geodesics and dominant intermediates. Geodesic pathways between each net and the cube computed using Eq. 1. The dominant intermediates are 1 and 5 in the third row. In this discrete model, nets 1, 3, 6, 10, and 11 fold through intermediate 1, and nets 2, 4, 5, 7, 8, and 9 fold through intermediate 5.

5. The role of pathways on self-assembly[*]

In previous chapter we noted that *the compactness determines the success of self-assembly*. However, in spite of choosing compact icosahedron nets ($Vc = 20$), it was not possible to self-assemble perfect icosahedra successfully. It can be concluded that the criteria of compactness alone may not be sufficient for self-assembly. Hence in this chapter, the research work aimed to investigate the role of self-assembly pathways and intermediates is detailed.

It was shown that the self-assembly of cubes proceeds through some preferred intermediates (**Figure 4.7**). In order to investigate it further, self-assembly pathways of dodecahedra formation were studied with theory and experiments. Since the dodecahedron has 43,380 nets, a much smaller set of nets was considered to obtain a manageable comparison with experiment. An exhaustive search through all 43,380 nets reveals that only 21 of these nets[55] have the maximal number of vertex connections ($Vc = 10$ in this case). All intermediates that originate in these nets were computed to find a poset with 2799 vertices that were called the restricted configuration space $\mathbb{R}$. First, using discretization of intermediate states, self-assembly pathways were modeled and then validated experimentally.

5.1 Modeling self-assembly pathways

The experimental observations of self-assembly in a discrete folding algorithm were termed as gluing at vertex connections.[34] A self-assembly pathway was treated as a discrete sequence of states $p = (S_0, S_1, \ldots S_n)$ between a net $N = S_0$ and the convex polyhedron $P = S_n$. While each state S_k is a collection of edges, faces and vertices, it is identified with the closure of its embedded image in Euclidean space for simplicity of description. The notion of folding and sealing hinges and vertex connections were generalized from the planar net S_0 to each state S_k: the edges on the boundary of S_k are called as sealing or locking hinges, and other edges between two panels as the folding hinges. A vertex on the boundary of S_k is called a vertex connection if it is shared by two panels that do not share any edges. The states S_k are generated in sequence from the state S_0 as follows. For each $k \geq 0$, a vertex connection v_k of S_k is chosen, and all locking hinges that meet at v_k are glued in pairs to form a state S_{k+1}. When gluing faces at locking hinges, the faces are only allowed to rotate rigidly through the dihedral angle about folding hinges that meet at v_k. The procedure terminates when the polyhedron is formed. This is termed as gluing. Thus all the states S_k obtained in gluing are called intermediates and the set of all these intermediates is the configuration space denoted by C.

5.2 Distance functions and intermediates

Since the states in C are embedded in $\mathbb{R}^3$, we assigned a cost $d(S_k, S_{k+1})$ to each edge between neighboring states $S_k, S_{k+1} \in C$ based on the distance traveled by faces in $\mathbb{R}^3$ as the polyhedral linkage S_k is transformed into S_{k+1} by gluing at a vertex connection.[34] It is

convenient to informally refer to the cost $d(S_k, S_{k+1})$ as the distance between S_k and S_{k+1}. The underlying heuristic idea here is that the energy dissipated when moving a panel scales linearly with Euclidean distance in an overdamped flow. Thus, the distance between the net and polyhedron serves as an easily computed proxy for the viscous energy dissipated along an assembly pathway, which incorporates the kinematic constraints of folding by rigid rotations about folding hinges.

First the distance between two surfaces that differ by a rotation is defined, and then extended this formula to a distance between two neighbors in C. Assume given a surface S that consists of a collection of polygons, an edge e that separates S into two polygonal surfaces Ω_1 and Ω_2 with common boundary e, and an angle of rotation θ. We define a new surface $\tilde{S}$ by rotating Ω_1 and Ω_2 rigidly about e through θ (**Figure 5.1**). In this process, each point on the surface Ω_i at a distance r from the edge e moves a distance $r\theta_i$ where $\theta_1+\theta_2=\theta$. The total squared distance traveled by surface Ω_i is then $\int (r\theta_i)^2 \, dA = I_i \, \theta_i^2$ where I_i is second moment of inertia. Then the cost of this move is defined as:

$$d^2(S, \tilde{S}) = \min_{\theta_1+\theta_2=\theta} I_1\theta_1^2 + I_2\theta_2^2 = \frac{I_1 I_2}{I_1 + I_2}\theta^2.$$

The transformation of a state S_k into a state S_{k+1} by gluing all faces at the vertex connection v_k consists of a number of sub-steps each of which involves a single rotation. The distance between S_k and S_{k+1} is defined by minimizing the distance over the set of possible surfaces between S_k and S_{k+1} that differ by the rotation of a single face. On minimization of the total distance $I_1\theta_1^2 + I_2\theta_2^2$ subject to the constraint $\theta_1+\theta_2=\theta$, distance between two

intermediates I and J is given by:

$$d^2(I,J) = \min \sum_{j=0}^{k-1} d^2(S_j, S_{j+1})$$

The above definition of d has the following important intuitive consequence: For fixedθ, $d(S, \tilde{S})$ is smaller if $I_1 \ll I_2$ than if $I_1 \cong I_2$. Thus, it costs less to fold a face on an extremity of S than to rotate two equally balanced domains 1 and 2. Hence, when computing shortest paths from a net to a polyhedron usually it was found that the faces on the boundary of S fold first, until no such moves are possible.

5.3 Conclusions

The results are shown in **Figure 5.2** and **Figure 5.3** along with a few experimental pathways for ease of comparison. From the snapshots of self-assembly process (**Figure 5.4**) it was found that all the greedy paths funnel through states that consist of two half dodecahedra linked by a hinge (states 2788, 2791 and 2797). Of these three, 2797 is the most important since 16 of the 21 nets funnel through it (**Figure 5.5**). These three states and 2797 in particular, are especially conducive to self-folding with no misfolding: each half-dodecahedron is rigid and the intermediate has a single rotational degree of freedom about the hinge. When the two halves meet, several edges lock into place simultaneously.

When compared with experiments, the greedy paths were found to replicate the experimentally observed pathways better (**Figure 5.6**). These computed pathways are a rough approximation of the true continuous pathway, and the experiments do not permit a

44

statistically reliable resolution of fine distinctions such as whether intermediate 2788, 2791 or 2797 best approximates the observed half-dodecahedra. Nevertheless, the trend towards such pathways is clear, as is the fact that the greedy paths are much better approximations to the observed pathways than the global geodesics. Thus it is important to note that the role of pathways is very important for the high yield of self-assembly.
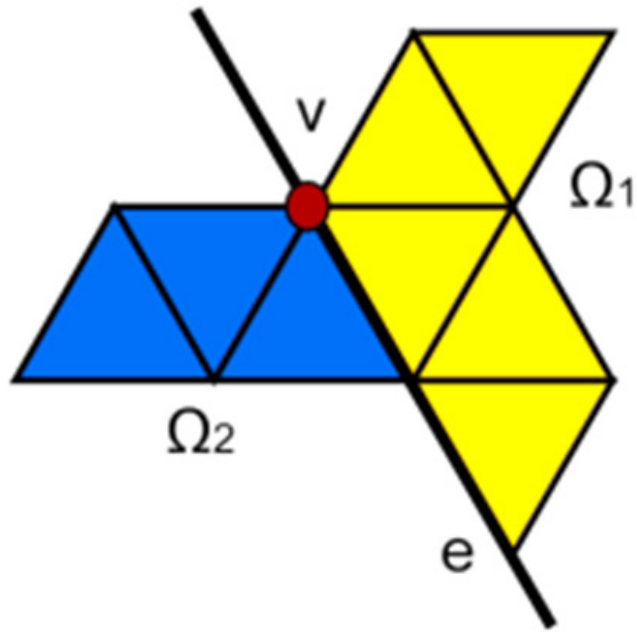
Figure 5.1 Transformation of an octahedron state S_k to S_{k+1} by rotating the surfaces Ω_1 and Ω_2 by θ_1 and θ_2 respectively.
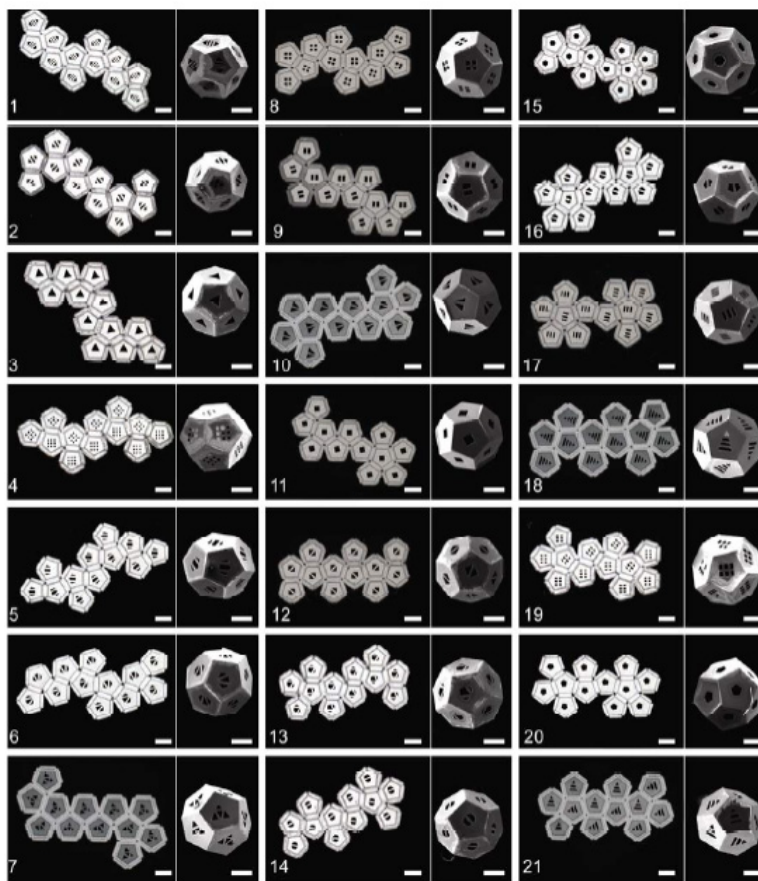
Figure 5.2 The 21 nets with maximal *Vc* and self-folded dodecahedra. Nets 1–21 are ranked in order of decreasing *Rg*. In each figure, the image on the left is an optical microscope image of the net. On the right is a scanning electron microscope (SEM) image of the self-folded dodecahedron. The scale bar is 300µm.
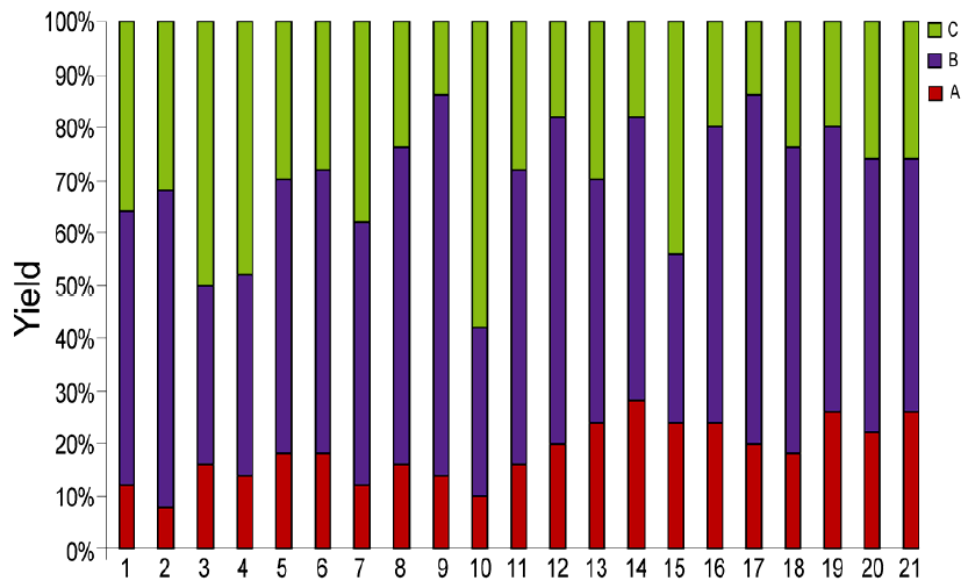
Figure 5.3 Yield of self-folded dodecahedra. Each self-folded polyhedron is examined visually and sorted into three grades. Grade A polyhedral have no visual flaws; Grade B polyhedra allow misfoldings by at most 20^0; Grade C polyhedra have faces that are misaligned by more than 20^0. Only comparisons that differ by more than 5% are statistically meaningful.
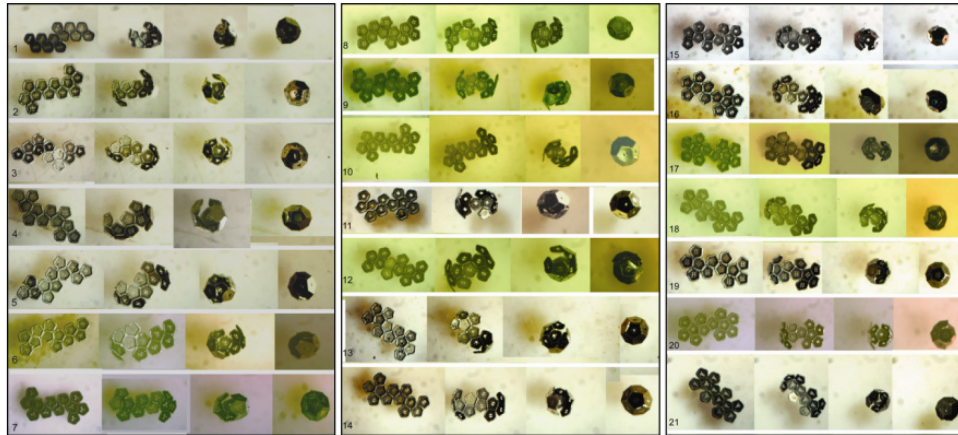
Figure 5.4 Snapshots of movies of self-assembly of dodecahedra nets. All 21 nets have same number of vertex connections, *Vc=10*.
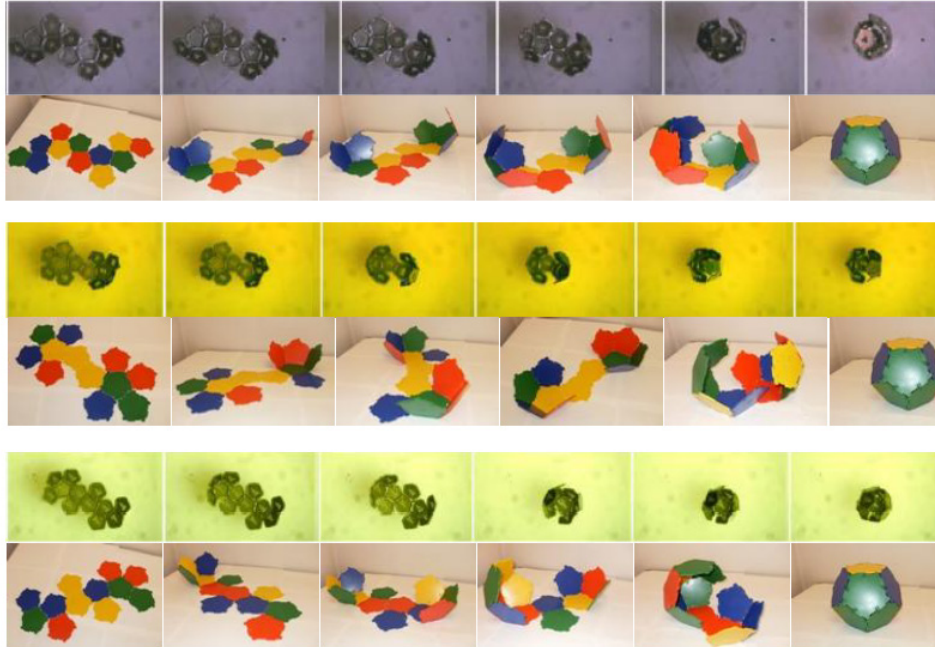
Figure 5.5 Greedy paths for the dodecahedron and comparison with experiment Upper: net 3; Middle: net 17 ; Lower: net 18 . Nets 3,4, and 5 pass through state 2788 (upper). Nets 12 and 18 pass through state 2791 (lower). All 16 remaining nets pass through state 2797 (middle).
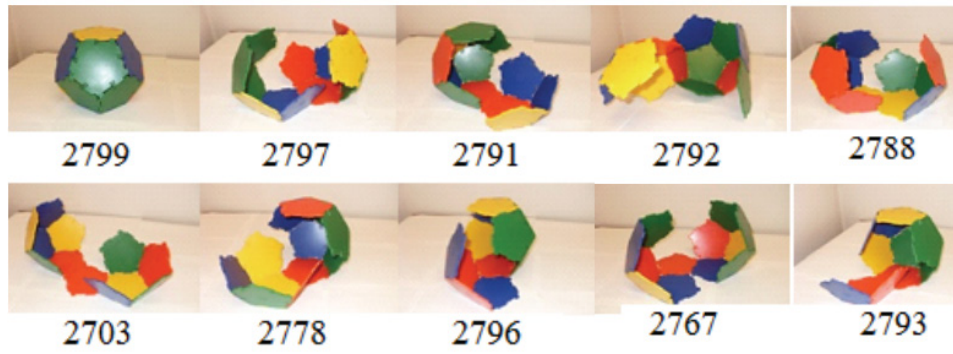
Figure 5.6 The 10 most prevalent states for the dodecahedron in decreasing order (2799 precedes 2788; 2788 precedes 2703).

6. Self-assembly of mesoscale isomers: The role of intermediates and the degrees of freedom[*]

Structural isomers are an important class of molecules with the same chemical formula but varied geometric arrangements of bonds, resulting in different physical and chemical properties.[56] While it has been empirically established that catalysts can be used to control the ratio of formation of different isomers in a chemical reactions[57, 58] the role of geometry, steric interactions in intermediates and assembly pathways are not very well understood. Consequently, mechanisms and rational designs to synthetically enrich one self-assembling isomer over the other are limited.

6.1 Formation of self-assembled polyhedral isomers

In this chapter, the self-assembly of isomers in a mesoscale model system has been investigated. Self-assembly is a technique to create higher order complex structures from multiple subunits. These subunits can be biomolecules, nanostructures or microscale and millimeter scale structures.[50, 59-66] Here, the mesoscale model involves the self-assembly of 300 μm sized polygonal units into polyhedra using surface tension driven forces that both fold

---

[*] Parts of this chapter have been adapted from Pandey S., Johnson D., Kaplan R., Klobusicky J., Menon G., Gracias D.H. "Self-assembly of mesoscale isomers: The role of pathways and degrees of freedom" *PLOS One* (2014).

panels and seal edges. It is important to note that this work is focused on the self-assembly of an octahedron, a Platonic polyhedron which can be constructed by folding a planar assembly of eight triangles termed a net as shown in **Figure 6.1**. Despite its simplicity, the octahedron was chosen for the study, because its nets can also be folded into a second non-convex conformation, akin to a boat, as illustrated in **Figure 6.1**. These two three-dimensional shapes have the same precursor, but are formed by different bonding arrangements between edges. Thus, they are structural isomers. In what follows, the (convex) octahedron is referred as Isomer I and the non-convex 'boat' as Isomer II. The formation of these isomers is investigated with theory and experiment and the degrees of freedom of intermediate states have been analyzed to demonstrate how a precursor can be manipulated to increase the yield of formation of Isomer II.

6.2 Experimental details

Using gluing algorithm as detailed in previous chapters, the configuration space $\mathcal{C}$ of self-assembly of all 11 octahedral nets were calculated. As shown in **Figure 6.2**, intermediate states linked with red lines are obtained from gluing at edges that subtend 120^0 of angle and they all lead to formation of Isomer I, whereas the intermediate states linked with green lines obtained by gluing at both exterior angles 120^0 and 180^0 lead to formation of Isomer II and some kinetically trapped states. Kinetically strapped states are the intermediates that are not completely closed 3D structures but are assembled in such a way that no further assembly is possible. The corresponding shapes are shown in **Figure 6.3**. Self-assembly experiments

(**Figure 6.4**) were performed and data statistically analyzed. Greedy pathways and geodesics were computed using distance functions detailed in Chapter 5.

6.2 Properties of intermediates of self-assembly pathways

It was observed that the self-assembly pathways proceed through certain rigid intermediates. Although the hinge material was optimized for formation of Isomer I but it was found that Isomer II formed as well. The formation of Isomer II was observed to be mainly because formation of a tetrahedral corner due to bonding at 180^0.

6.3 Controlling self-assembly pathways to enrich one isomer over the other

Since it was observed from the self-assembly movie (snapshots are shown in **Figure 6.5**) that the partial rigidity of intermediates and the associated pathways were important in determining which isomer self-assembled, it was hypothesized that it might be possible to selectively enrich the formation of one isomer over the other by manipulating these geometric criteria. Importantly, it was observed that Isomer II formed through rigid intermediates formed only via 180^0 folds, relative formation of isomers from two identical nets (Net 10, **Figure 6.6**) was experimentally compared with just one difference. Essentially, one panel that is important in maintaining rigidity of partially folded modules of intermediates via 120^0 folds was omitted and the self-assembly yields were compared. In essence by removing this panel, it eliminates two vertex connections and reduces the degrees of freedom of the partially folded intermediate

54

in the first tier (S_1). Consequently, the pathway that occurs during the delay in rotation of the outer panel was biased.

This hypothesis was tested experimentally. After self-assembly of a sample set of 50 for each of the two nets shown in **Figure 6.6**, the polyhedra were carefully examined under an optical microscope and categorized into three grades: grade A with no defects observed under the microscope, grade B with panels misaligned by an angle of 20^0 or less, and grade C includes polyhedra with multiple defects. Remarkably, the fraction of perfect isomeric polyhedra was dramatically different for the two cases. Even though the geometric placement of the panels in the net is identical, just by removing this one panel, the yield of A grade Isomer I decreased by a factor of two and simultaneously the yield of A grade Isomer II increased by a factor of six (**Figure 6.7**). As depicted in this figure, on removal of the panel, the pathway with intermediates 30 and 32 is enriched over the pathways with intermediates 12, 16 and 22. This experiment highlights how the degrees of freedom of intermediates and the pathways can be engineered by manipulating the geometric constraints of initial precursors to enrich one isomer over another.

6.4 Analogies with chair-boat transition of cyclohexane

Some of the earliest studies directed at explaining the formation of the two isomers of cyclohexane used paper origami[67]. In order to relate this work to this fundamental example in stereochemistry, it is important to revisit the conformational analysis of cyclohexane from the point of view of the theory of linkages. Here, two ideal linkages are compared: a polyhedral

linkage that can be folded into Isomers I and II as in this model experimental system, and an ideal geometric model of cyclohexane.

Cyclohexane (C_6H_{12}) is a molecule composed of six carbon and twelve hydrogen atoms. The carbon atoms are connected in a ring with two hydrogen atoms attached to each carbon atom. Each carbon has four bonds that energetically prefer spacing at tetrahedral angles. While the actual configurations of cyclohexane balance various effects such as eclipsing strain, angle and steric crowding, Sachse's ideal geometric model was used to facilitate a comparison with polyhedral linkages. It was found that the chair has zero degrees of freedom whereas the boat has one. This means that it is impossible to transform the chair into any other configuration without deforming the bond lengths or angles. It should be noted that this is a purely kinematic argument for the greater stability of the chair form of cyclohexane. However, since the boat has one degree of freedom, it can be deformed continuously while keeping the bond lengths and bond angles fixed. Three such intermediate configurations are shown in **Figure 6.8** (Boat 2, the twist boat and the twist chair). Of these configurations, the twist chair is closest to the chair. In Sachse's ideal geometric model, the chair is rigid; therefore it cannot transition into the boat. In reality, thermal effects allow fluctuations in bond lengths. To transition between the chair and boat configuration, the chair model must first become a twist chair and then a twist boat before it can finally become boat 1 or boat 2. Similarly, to transition between two boats, the twist boat intermediate must be visited.

For the analogous transformation of the octahedron between Isomer I and Isomer II, it is necessary for an edge to break (unfold), the linkage to move, and the edges to refold. This can occur along many pathways (Figure 6.2) and one such example is shown in Figure 6.8B. At present, the gluing of hinges in this model experiment is irreversible. Nevertheless, the analogy between these two polyhedral systems suggests that it is possible for octahedral isomers to transition from one to another by choosing appropriate (flexible) hinge materials and mechanical agitation.

6.5 Conclusions

A mesoscale experimental model and the theory of polyhedral linkages have been used to study the self-assembly of structural isomers, and to design an experiment that demonstrates the preferential enrichment of one isomer over the other. In this chapter an important finding of relevance to self-assembly systems has been reported as: the pathways that proceed through intermediates with favorable rigidity dominate the self-assembly process. It was shown how isomer enrichment can be achieved by manipulation of the degrees of freedom of initial precursors using purely geometric criterion to bias specific assembly pathways. It was achieved by the removal of a panel and consequently two 120° vertex connections so that the rotation sequence of panels could be controlled to follow pathways leading to Isomer II. Steric and geometric manipulations of molecules are known to be important in molecular catalysis and these ideas are in agreement with findings. These findings also suggest that the design of systems that alter the degrees of freedom of precursors

and intermediates are important in synthetic self-assembly. The development of approaches to search for and design rigid or stable intermediates could prove useful in solving many inverse problems in self-assembly. Consequently, steric hindrances or more rigid geometric additions could be included to design synthetic self-assemblies that can be guided to follow a pathway to preferentially form a specific outcome out of many possible outcomes; the latter being a hallmark of biological and natural self-assembly.
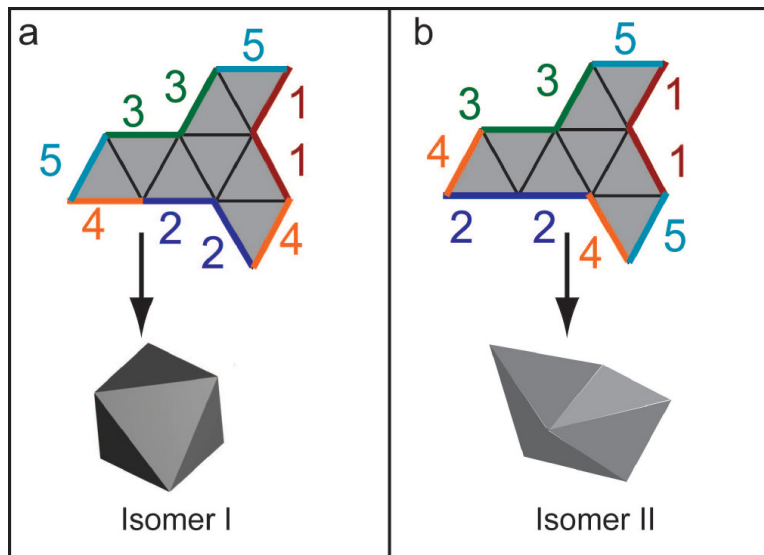
Figure 6.1 Schematic illustration of the self-assembly of two different octahedral isomers from the same initial precursor or net. (a) Isomer I is a convex octahedron, while (b) Isomer II is a non-convex octahedron. Both form from the same precursor net but when different edge pairs denoted by 1, 2, 3, 4, and 5 meet. In Isomer I, each vertex is bonded to four other vertices through edge connections whereas in Isomer II, two vertices have four edge connections, two have five and the remaining two vertices have three edge connections.
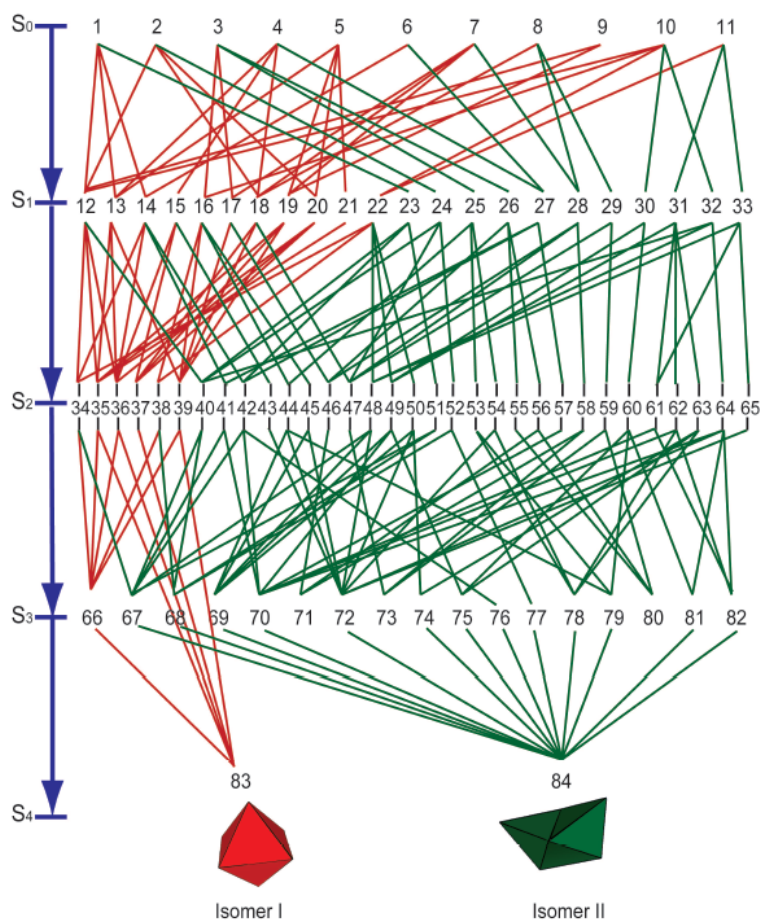
Figure 6.2 The extended configuration space C for the octahedron showing intermediates and transition states. The paths in red correspond to states linked by gluing at vertex connections with exterior angle 120^0 (configuration space R) and the paths in green link states obtained by gluing at both types of vertex connections. The extended configuration space includes four new terminal states: state 84 is the non-convex boat, and states 71, 73 and 80 are kinetically trapped states.
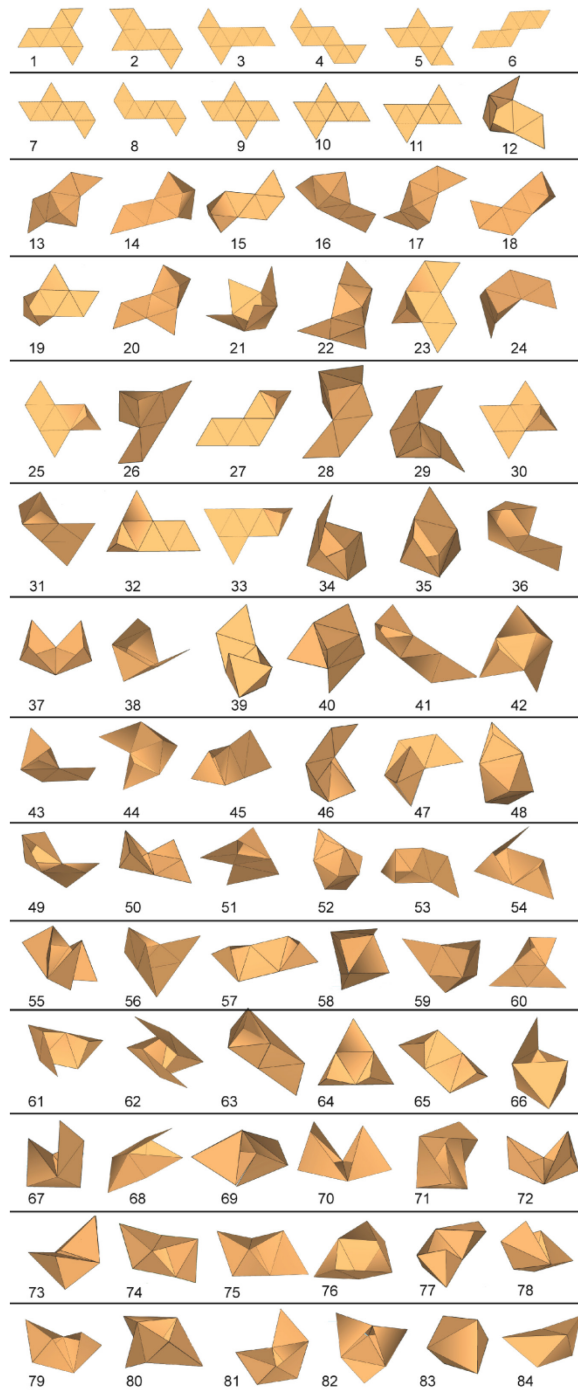
Figure 6.3 Shapes of all 84 states of configuration space of octahedral assembly.
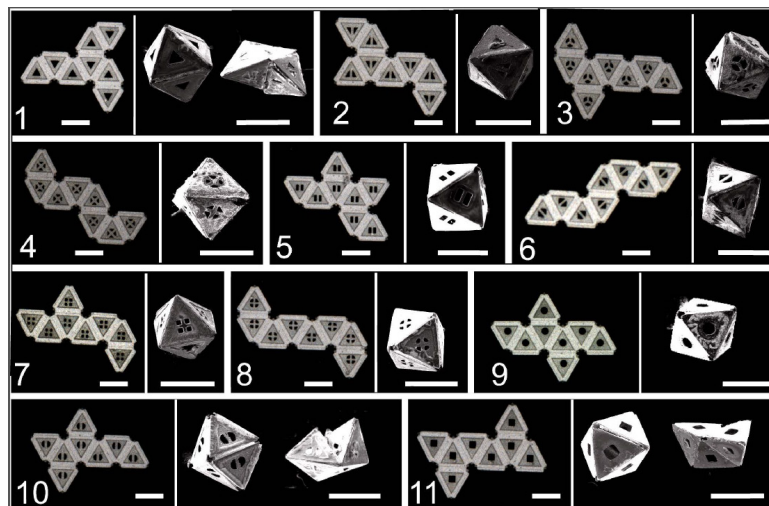
Figure 6.4 Experimental result of self-assembly of octahedra**.** Optical (left) and scanning electron microscopy (right) images of all 11 octahedron nets and their self-assembled isomers; Isomer I (83) and Isomer II (84). The scale bar is 300 μm.
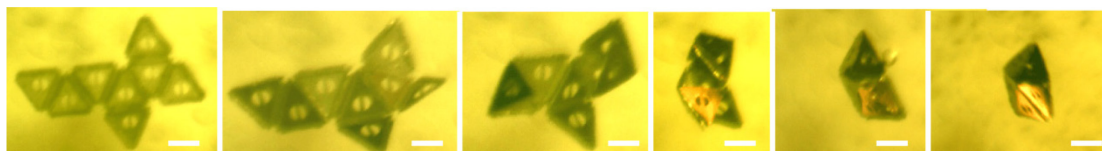
Figure 6.5 Snapshots of self-assembly of octahedron net 10 into Isomer II. Scale bar: 300 µm.
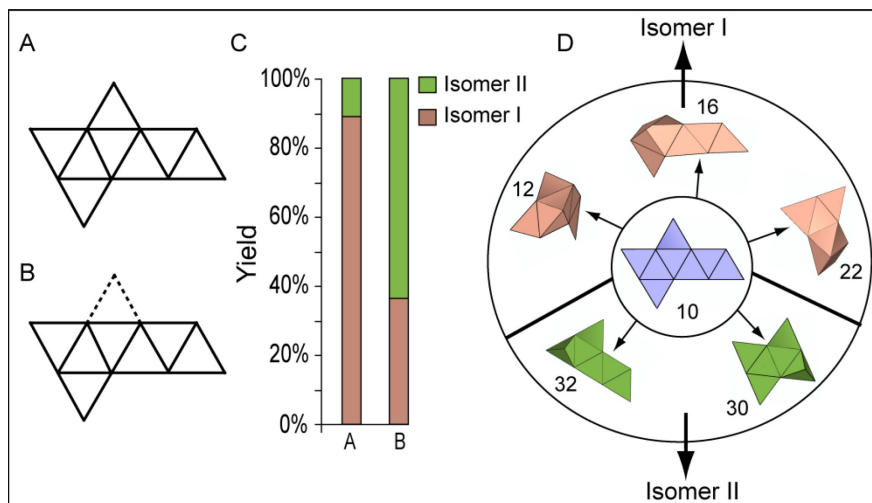
Figure 6.6 Geometric manipulation of identical precursor nets to manipulate pathways to enrich an isomer. The net 10 shown in (a) and (b) have identical placement of faces but a single face indicated by the dotted line is excluded to enhance pathways which feature a propensity for 180^0 folds. (c) Experimentally obtained yields showing a dramatic increase in Isomer II and decrease in Isomer I for the engineered net. (d) Images of precursor net and pathways which feature intermediates (shown in green color) leading to Isomer II, are enriched for net b as compared to net a.
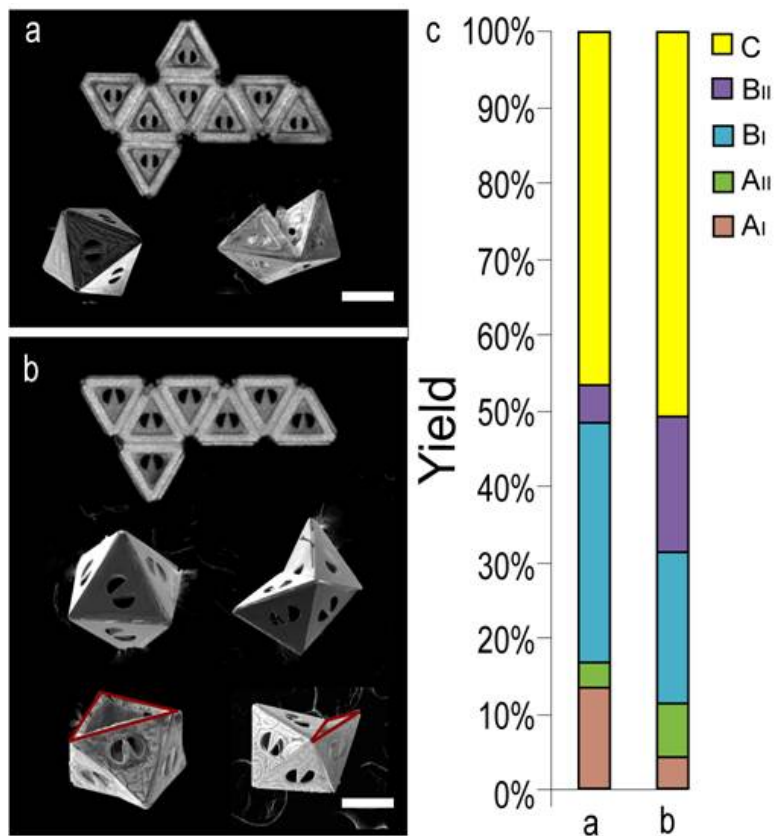
Figure 6.7 Engineering self-assembly pathways by manipulating design constraints to enrich formation of Isomer II. (a) optical image of octahedron net 10 and SEM images of self-assembled isomers I and II; (b) optical image of an engineered net identical to net 10 but one outer panel removed and SEM images of self-assembled isomers I and II. The red triangles represent the open face because of the removed panel; (c) relative yields of isomers I and II formed from the octahedron nets shown in (a) and (b). The scale bar is 300 μm.
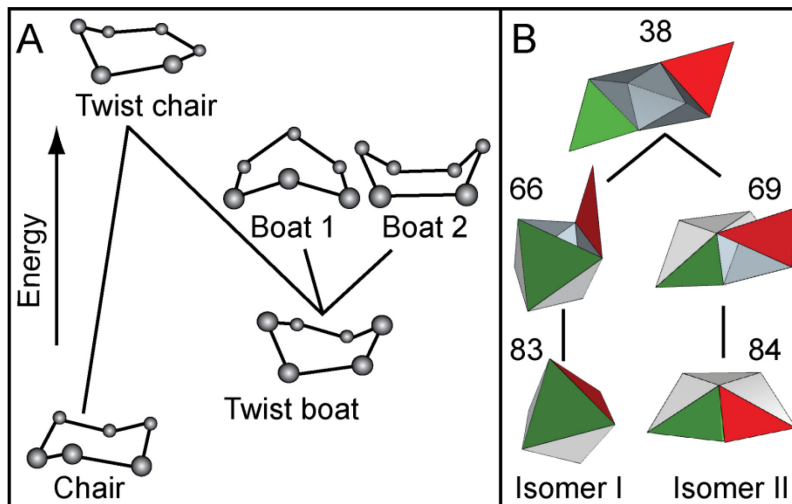
Figure 6.8 Analogy between (a) pathways of chair/boat transition of cyclohexane and (b) an example of pathways for transition between octahedral isomers I and II. Boat 1 and Boat 2 have same geometry but differ by which of the six carbon atoms form front and back tips of the cyclohexane ring.

7. Polymeric micropolyhedra by folding and molding[*]

Polymeric microparticles are very important for variety of applications such as drug delivery,[68-72] cell encapsulation for tissue engineering,[73-77] biomaterials for biomedical applications [78-80] as well as for the fundamental studies in the fields of microfluidics,[81] and colloidal self-assembly.[82-84] Functional behavior and interparticle interaction between polymeric microparticles strongly depend on their sizes and shapes, consequently making polyhedral particles attractive for self-assembly applications.[85]

There are numerous advanced methods such as molding, micromolding in capillaries,[86, 87] microinjection,[88-90] and microfluidic methods,[91] to create various types of microstructures with sizes ranging from micro to the millimeter length scale but these methods are generally limited mostly to simple geometries such as spherical, cylindrical, conical, and ellipsoidal shapes.[92-97] For example, polymeric particles in spherical shapes are the most studied objects for colloids, drug delivery, self-assembly and biomedical applications as the spherical shapes can be readily synthesized in a high throughput manner with existing methods.[98-103] Moreover, there is a need of polymeric microparticles of different polyhedral shapes for their use in the studies on phagocytosis,[104] drug delivery,[105] self-assembly and tissue engineering.[106] It has been shown that phagocytosis by cells depends on the shape of particles where internalization of some shapes are preferred to others.[104, 107, 108]

---

[*] Parts of this chapter are edited excerpts from Pandey S., Yoon C.K., Kwag H.R., Zhang Z., Gracias D.H. "Soft polyhedral by folding and molding", in preparation.

So far most studies on colloidal assemblies have been conducted with spherical particles which have the most basic shape.[109-113] It is important to note that two spheres can interact only at a single point which does not reflect any directionality in orientation, whereas polyhedral shapes such as cubes, dodecahedral and octahedral shapes can interact with their surfaces. Surface to surface interaction can occur in many ways such as partial overlapping, complete overlapping, and angular orientation with different angles of overlapping,[114] resulting different distributions of surface forces which could contribute to different colloidal properties. One of the main reasons that the effect of polyhedral shape on colloidal properties could not be explored much is because it was not possible to make different shapes using existing methods. Synthesis of polymeric polyhedra poses two main challenges: (i) precise control of size and shapes, and (ii) mass producibility. It has been previously demonstrated that self-folding process can be used to synthesize hollow polyhedra with varying sizes and shapes with polymeric materials.[36] It is a highly versatile method to create different shapes and sizes of micropolyhedra and precise patterns could be defined as well. On the other hand, micromolding is a relatively easier process to synthesize microparticles of different geometries. Molding has been very successful for making complex-shaped particles with a range of materials at nano and microscale but precise patterning on the surfaces of the particles has not been shown previously due to a limitation of transferring the patterns onto the inner walls of the mold itself.

Here in this chapter a method has been detailed that combines self-folding methodology with existing molding methods to address the need of a mass producible process for creation of complex-shaped polyhedral microparticles with precisely patterned surfaces.

Self-folding methodology enables us to create large number of metallic or polymeric particles with any desired size, geometry and patterns in a parallel process. In this process, the patterned 2D templates are heated above the melting temperature of the hinge materials and the templates self-fold to form perfectly sealed 3D nano- and microparticles of any size, shapes, and patterns with precision.[35, 37] These metallic particles are used as master particles to prepare PDMS molds where molds have precise patterns on the inner walls.

7.1 Experimental details

This method of combining molding with self-folding process not only enables to make complex-shaped microstructures but also makes it possible to transfer arbitrary patterns precisely onto the surfaces of the molded particles (**Figure 7.1**). First, self-folding methodology is utilized to create metallic polyhedral structures with precise size, shapes and patterns on their surfaces that were used as the master for casting PDMS molds. These metallic polyhedral structures can be used repeatedly for casting molds. After casting molds, patches patterned on the surfaces of master polyhedra transfer to the interior surface of molds prepared with PDMS. After PDMS has been cured the mold are filled it with different photocrosslinkable and chemical crosslinkable polymers and crosslinked them. After crosslinking the molded polymeric polyhedral are released from the PDMS molds. A schematic illustration of the process is shown in **Figure 7.2** and **Figure 7.3**. The molds prepared in PDMS can be used repeatedly over several cycles of molding process. This method can be utilized to synthesize different shapes of polyhedral shapes such as tetrahedra, cubes, dodecahedra and truncated octahedra with a variety of epoxy polymers and hydrogel

materials such as NOA 73, PEGDA, NIPAAM, and iron oxide mixed polymers. Also, synthesis of cell laden hydrogel can be used as bioblocks for tissue engineering applications where different polyhedral bioblocks can be used to build organized 3D structures. Building an organ with microscale and mesoscale blocks using soft lithography and molding has been widely reported.[115, 116] Here, molded mesoscale polyhedra with beta pancreatic cells embedded and molded into the shape of a pancreas has been discussed.

7.1.1 Fabrication of self-folded polyhedral micropolyhedra:

Master polyhedral shapes were synthesized via surface tension driven self-assembly method as discussed earlier.

7.1.2 Preparation of PDMS molds:

PDMS elastomer kit (Dow cornings) was used for mold preparation. First the base part and the curing agent in a 10:1 (w/w) ratio were mixed vigorously using a plastic spatula. This mixing process resulted into a large number of bubbles. To remove the bubbles, the mixture was placed in a desiccator for 30 min. After 30 minutes of desiccation all bubbles were removed and a thick clear liquid was left.

The metallic polyhedra were attached onto a double sided tape that was secured to the bottom of a petri dish. This prevented the floating of the structures when PDMS were poured into the petri dish. The elastomer solution was gently poured into the petri dish until it

completely covered the master polyhedra and placed the petri dish in a desiccator again for 30 min to remove any bubbles present and cured the elastomer solution at 50 ^{0}C for 4 hours. The solidified PDMS was gently pealed off the substrate where the metallic polyhedra remain attached on the tape thus creating molds with the shape of the structure.

7.1.3 Molding of polyhedra

Polymeric polyhedral were molded of various shapes made of different materials, e.g. NOA73, PEGDA, and PNIPAM. A variety of molded polyhedral have been shown in **Figure 7.4**.The solutions were spread on the molds and since there is a strong interfacial force that prevents the liquid from filling the small space, it was placed in a desiccator under vacuum for 2 hours. This step facilitated the liquid to go into the small molds and also removed any bubbles present in the solution. Once the molds were completely filled with the photosensitive polymer solution, it was exposed under the UV light for 3 min to crosslink the polymer.

7.1.4 Molding of cell laden polyhedra

Mouse pancreatic cell β -TC-6 was cultured in complete growth medium containing Dulbecco's Modified Eagle Medium with 10% fetal bovine serum. In the photoencapsulation process, first cells were stained with Calcein AM (0.7 ug/mL) in PBS solutions for 30 min in the incubato r(37 ^{o}C, 5.0% CO_2), then trypsinized and centrifuged at 1200 rpm to form a pellet. The pellet was suspended in 1 mL of PBS and 4 mL of PEGDA (700 MW), and Irgacure 2100 was added. The cell-PEGDA solution was spread on a sterilized PDMS mold

and exposed to UV for 2 minutes. After cross linking pancreatic cell-laden bioblocks of different shapes were released from the mold (**Figure 7.5**).

7.2 Conclusion

In this chapter a method of synthesis of different polyhedral shapes of different polymers was detailed. It was also shown that the method could be used to create variety of bio blocks for potential engineering in tissue engineering and organ development.
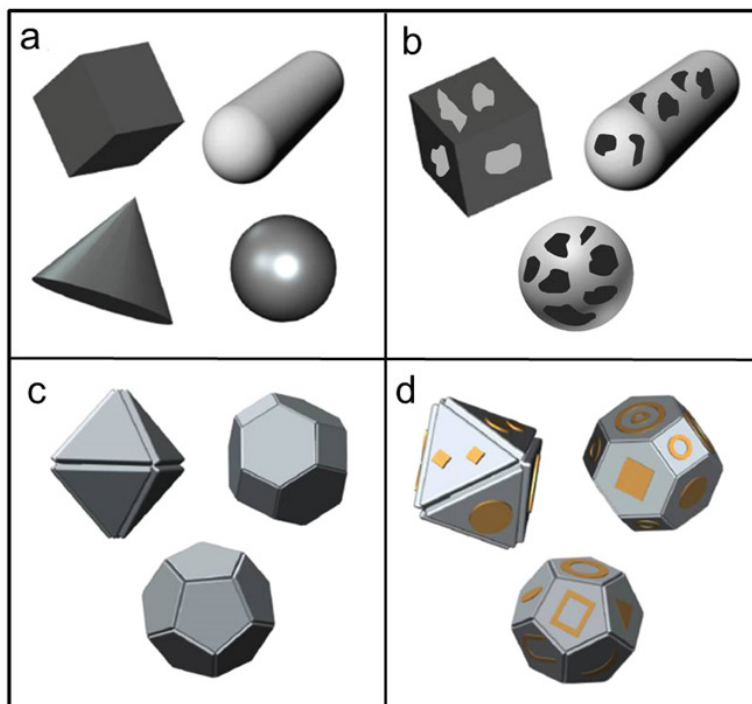
Figure 7.1 Schematic depicting limitations of current molding processes. (a-b) It has been shown that molding can be used to fabricate simple shape particles such as cubes, spheres, and cylinders at micro and nanoscale with patterns on the surface but it has not been possible to mold complex shapes such as dodecahedra and truncated octahedra with precise patterns. (c-d) With Our approach of combining self-folding and molding methodologies we can not only create complex microparticles of complex shapes (c), we can also define any arbitrary patterns precisely on their surface (d).
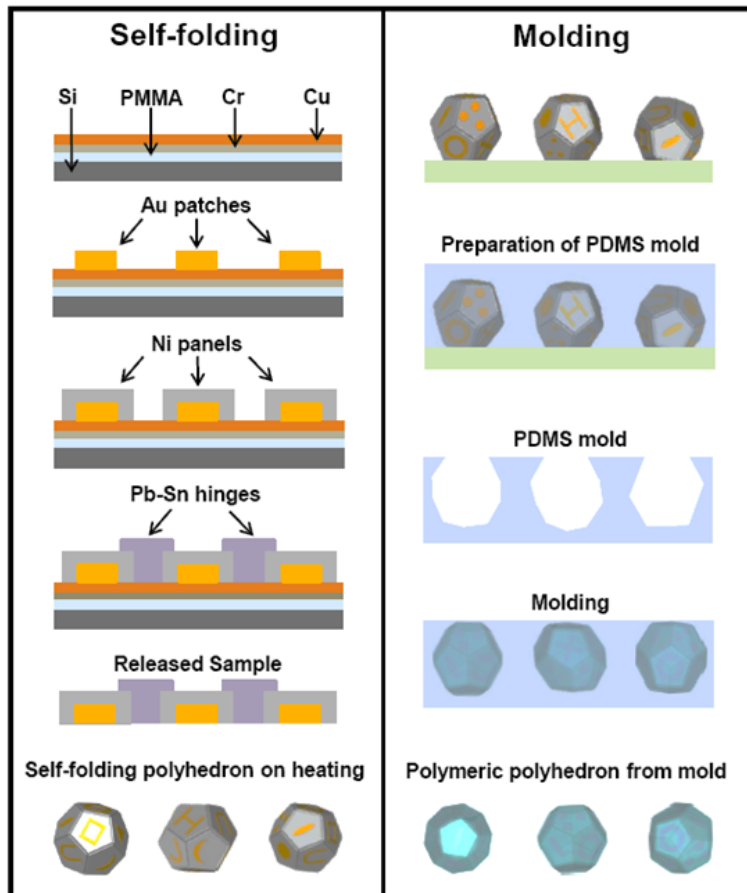
Figure 7.2 Schematic illustration of self-folding and molding processes. (A) Fabrication steps of self-folding patterned polyhedra used as master microparticles for making molds; (B) preparation of PDMS molds and creating polymeric micropolyhedra by molding.
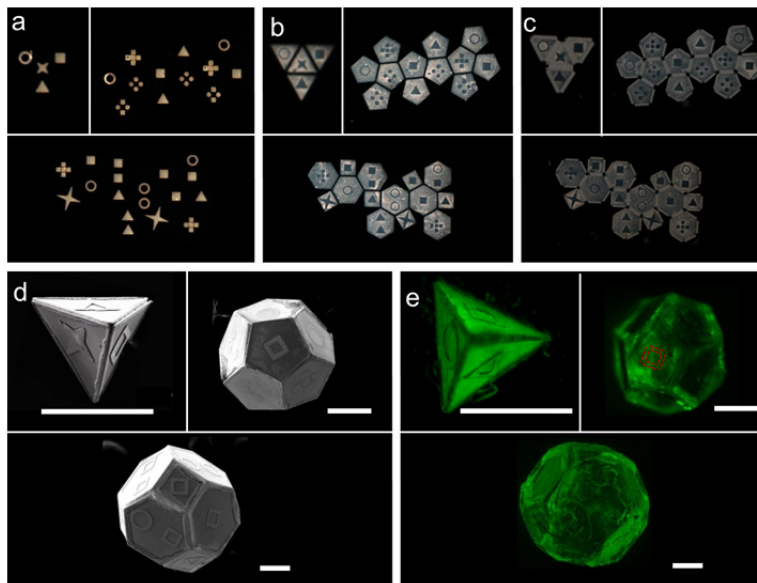
Figure 7.3 Process flow of self-folding combined with molding process. (a-d) Self-folding of metallic polyhedra used as master for making molds. Optical micrograph of lithographically patterned (a) gold patches, (b) Ni panels on top of the patches, (c) soldered panels; (d) SEM micrograph of self-folded pathcy polyhedra; (e) molded polymeric micropolyhedra stained with fluorescent dye. Scale bar: 300 microns.
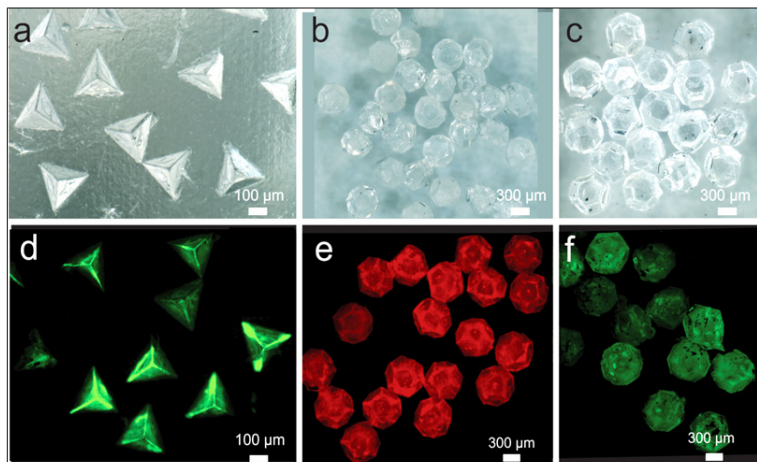
Figure 7.4 Mass producibility of complex shape micropolyhedra of different polymers. (a) Molded NOA73 tetrahedra with patterns, (b)molded dodecahedra with patterns, (c) molded truncated octahedra without patterns, (d) fluorescein stained molded PNIPAM tetrahedra, (e) rhodamine stained PEGDA dodecahedra, (f) Magnetic polyhedra by molding iron oxide mixed PEGDA hydrogel.
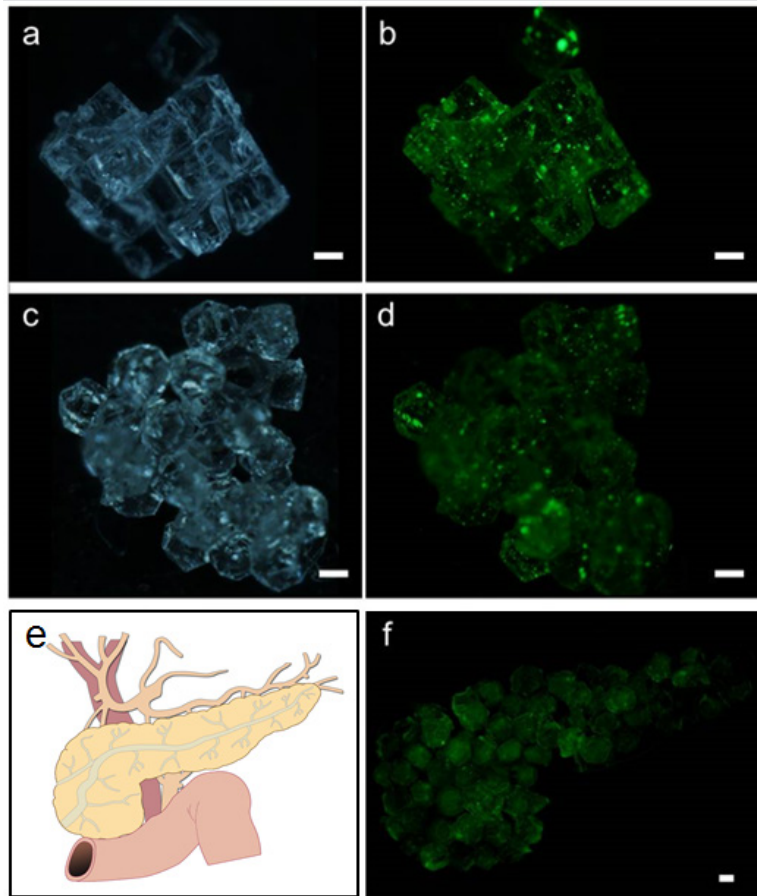
Figure 7.5 Molding of cell-laden bioblocks. (a) and (c) are optical images of cell-laden cubic and dodecahedral shape respectively and (b) and (d) are corresponding fluorescent images, (e) a schematic illustration of the structure of pancreas, (f) fluorescent image of a pancreas by self-assembly of dodecahedral bioblocks. Scale bar: 300µm.

8. 3D Computational devices by polyhedral E-blocks[*]

Computational elements are inherently in 2D. In order to enhance the computational speed of a device, a large number of computing elements are required. However, without miniaturizing the components it would not be possible to maintain an appropriate size of the device with enhanced computational capacity. With the development of high throughput miniaturization techniques now it is possible to fabricate computing componets as small as a few nanometers in size but there is a physical limit on it beyond which it is not possible to miniaturize these components. In order to make complex network of plaar electronic elements, interconnects become larger that results into power loss through interconnecting wire [117, 118]. There are approaches to make 3D micrhips by stacking such as monolithic technique, wafer-on-wafer, die-on-wafer and die-on-die stacking technique [119-124]. This stacking method has several advantages such as reduction of interconnects, high transistor density, complex networking that reduces power consumption and enhances the computational operation speed [125].But the stacking of several layers poses significant technological challenges in terms of precise alignment of layers, excessive heat generation between layers, yield, size effect and high cost of patterning. Here, we describe our approach of assembling polyhedral E-blocks in a three-dimensional space such that on a given surface we have higher density of computing elements. We use polyhedral E-blocks to control assembly into desired cellular architechture. Fabrication of 3D devices by self-assembly has been demonstrated for displays, functional electrical cirtuits and metamaterials [126-128]. Using polyhedral E-blocks is also enables us to

introduce porosity that will minimize the heating of components in the 3D structure. This approach involves (a) an algorithmic design of a self-reconfigurable defect tolerant toolchain for routing the power and signals, (b) mapping circuit diagram for polyhedral E-blocks from 3D to 2D and fabrication of E blocks from 2D circuit diagram, and (c) assembly of E-blocks to create a cellular architecture in 3D. A schematic illustration has been shown in **Figure 8.1**.

8.1 Designing 3D cellular architecture

8.1.1 Implementation of Cell-Matrix toolchain

We extended the concept of Cell-Matrix in 2D and 3D as introduced earlier. Briefly, it is a self-reconfigurable, fault tolerant electronic networking that can test the unit E-blocks for their functionality and self-reconfigure and self-modify accordingly. The fact that this toolchain is easily scalable and can be extended from 2D to 3D is very important in case of polyhedral E-blocks. For example, in the case of cubic E-blocks, the units can interact with six neighbors whereas in case of dodecahedral E-blocks, one unit can interact with 12 neighbors. Thus Cell-Matrix can easily be applied for polyhedral assembly (**Figure 8.2**).

8.1.2 Fabrication of polyhedral E-blocks

Polyhedral units have been previously used for forming self-assembled functional electrical connections, metamaterials and for terahertz applications. Polyhedral building blocks have several adtanges such as (a) assembly of units can be made symmetric and asymmetric depending on the kind of polyhedral shape we use, (b) porosity in assembly can

be included, (c) complexity of network can be controlled by designing the connections through faces, (d) E-blocks can be equipped with variety of components such as LEDs, sensors and microchips, (e) polyhedral shapes are mass-producible using lithography and self-folding techniques. Design principle and fabrication methods are as follows:

Here we focus our study on cube shape E-blocks. In order to fabricate cubic E-blocks, first, we mapped each layer of 3D circuitry diagrams (ciruit diagram for power, ground and signal as represented by VCC, GND and SIG in Figure 1) and printed on transparency films to make photomasks. For each layer of circuitry, we spincoated a photoresist (S1827, Rohm and Haas) at 3000 rpm onto a sheet of flexible copper-clad laminate (Pyralux® FR 9110R, Dupont) and baked at 115 ^{0}C for 1 min. We exposed photoresist coated sheets to UV light (365 nm) at ~180 mJ/cm^2 through respective negative masks with the features of wires and connectors for each VCC, GND and SIG layer, developed in a developer (Microposit 351 developer, Rohm and Haas) for 30 sec, etched off the exposed copper in an aqueous solution of ferric chloride (1.4 g/ml), rinsed the patterned sheets with DI water and dried with N_2 gas. Unexposed photoresist was removed by acetone. After patterning these circuit layers, we cut them out, aligned one on the top of the other, and attached a 4 mm x 4 mm PIC16F1827 microchip and folded into a shape of cube. We mounted these folded layers onto the cubes and completed the connection (**Figure 8.3**).

8.1.3 Computation results by E-blocks

In order to test the E-blocks the experiments required use of a testbed driver, which performs three functions:

1. it allows a host Linux machine to send 1s and 0s to the C and D inputs of the cells being tested, and for outgoing bits (generated by the cells) to be displayed on a series of LEDs;

2. it also allows the driving program to be disconnect ed, so that external hardware can supply the 1s and 0s to the cells being tested; and

3. It handles the time-multiplexing of D and C inputs and outputs (and clock signals) through the single-conductor SIG contact on each face of the e-blocks.

For a simple test, a single block was configured as a two-input OR gate. The inputs were driven by a function generator, and the output observed on an ocilloscope. The two inputs are on top (yellow and blue), and the output is on the lower trace (purple). The block performs perfectly, implementing the OR and AND functions. For more-complex tests, a logic analyzer was used to record multiple outputs under specific combinations of inputs (**Figure 8.4**). A complex hierarchical assembly has been shown in **Figure 8.5**.

8.2 Conclusions

In this chapter an approach of building 3D computational devices using folded polyhedral E-blocks has been outlined. The initial computational results show that the assembly method can be used to manufacture E-blocks of polyhedral shapes with desired circuit layers on it and assembled to make a functional device. In this case, although the E-blocks are of millimeter scale but the self-assembly process explained in this thesis could be used to fabricate miniaturized E-blocks.
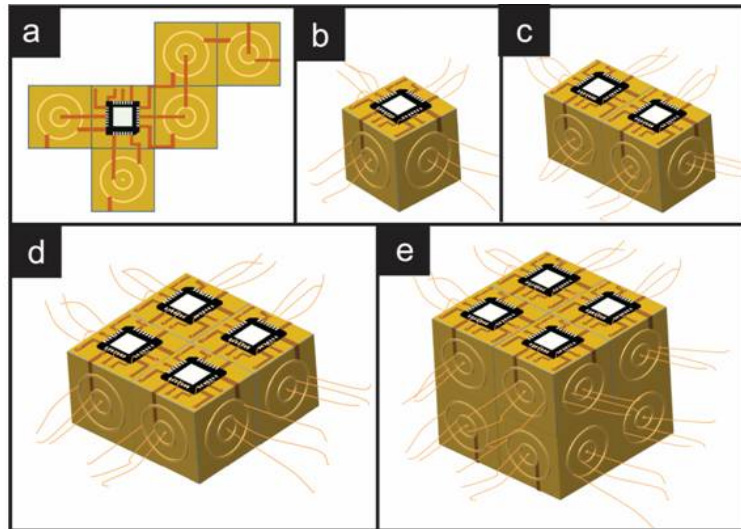
Figure 8.1 Schematic illustrations a self-assembled 3D computational device. (a) Two dimensional mapping of the circuitry designed for a three dimensional E-block, (b) folded E block monomer and (c) a higher order assembly of E block monomers.
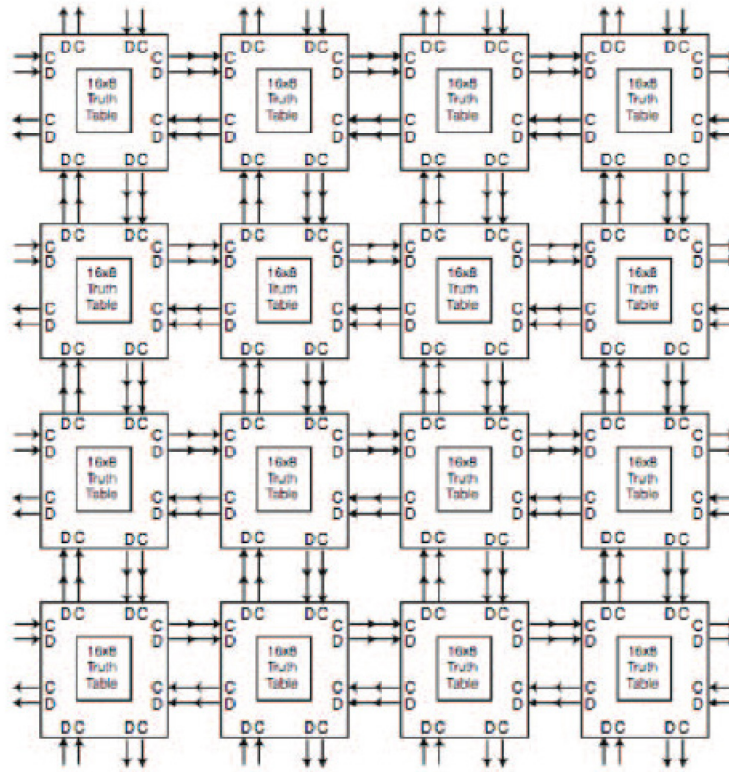
Figure 8.2 A scheme of cell-matrix concept.
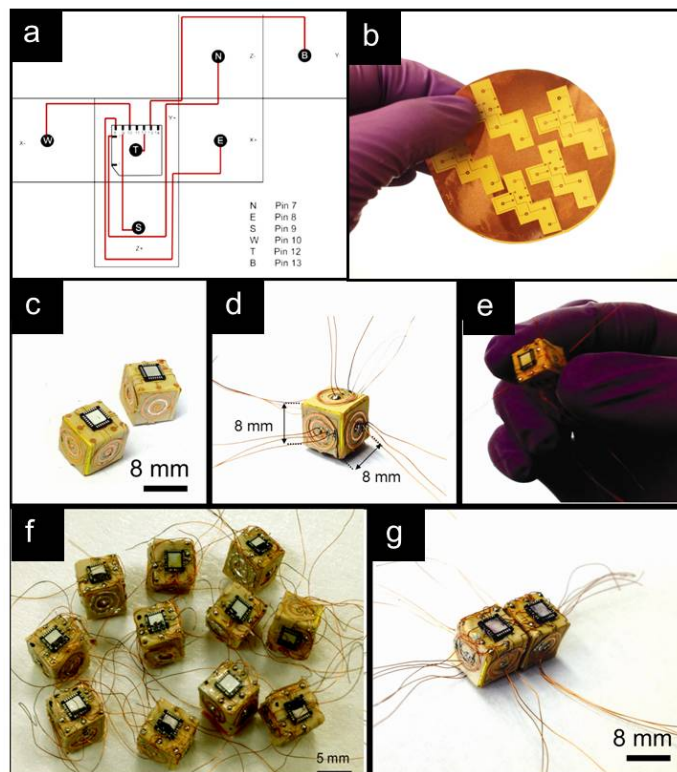
Figure 8.3 Fabrication steps of millimeter scale E-blocks. (a) 2D mapping of the circuit (signal layer) and connections to the pins of the microchip. Similar mappings were done for power and ground circuits, (b) lithographically patterned circuit diagrams on a flexible sheet, (c) the 2D maps of the circuits were cutout, folded into 3D and mounted on a cube, (d-f) finished E block monomers with connections, (g) a dimer of the E blocks with 'East' of one monomer connected with the 'West' of the other.
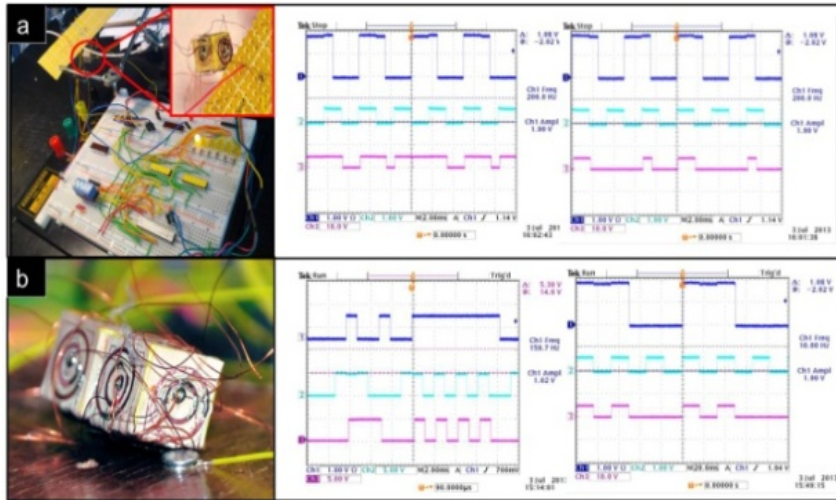
Figure 8.4 Testing of monomers and dimers of the E-blocks. (a) An E-block monomer on the testing setup, oscilloscope readings showing the output of the monomer configured as OR gate (center) and AND gate (right); (b) a dimer on the testbed and oscilloscope readings showing the dimer configured as a D latch.
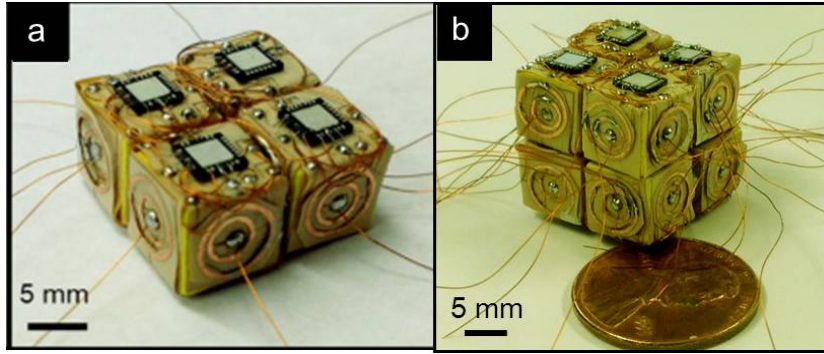
Figure 8.5 A higher order assembly of E blocks. (a) an image of a 2x2 assembly and (b) 2x2x2 3D-assembly of E blocks.

9. Summary and Future outlook

The work presented in this focused on a detailed study of self-assembly process from 2D templates to 3D structures and uncovering geometric design rules that govern self-assembly process. I investigated the formation of different structural isomers in synthetic self-assembly systems and developed an approach of how the formation of a desired isomer can be enriched over the formation of other isomer simply by manipulating geometric design rules. This approach presents a new perspective of studying isomeric molecules.

The folding and molding approach to create polymeric micropolyhedra of different sizes, shapes and materials presents a methodology that could be useful for tissue engineering and organ development applications. Making these polymeric polyhedral smaller would help study colloidal behavior of polyhedral microparticles. It should be noted that most of the studies on colloidal behavior have been limited to simple shapes such as microsphere, discs, and cylinders.

The concept of polyhedral E-blocks discussed in the last chapter of thesis presents a novel approach toward building 3D computational architecture. So far, computational elements have either been planar or quasi three dimensional. Whereas this method could be used to control porosity of architecture, robustness, and packing density that will consequently increase computational speed and minimize heating of the elements.

References

1.   Cromwell, P. R., *Polyhedra*. Cambridge University Press: 1999.

2.   Malkevitch, J., Milestones in the history of polyhedra. In *Shaping Space*, Springer: pp 53-63.

3.   Knutson, A.; Tao, T., Honeycombs and sums of Hermitian matrices. *Notices Amer. Math. Soc* **2001,** 48, (2).

4.   Williams, R. C.; Smith, K. M., The Polyhedral Form of the Tipula Iridescent Virus. *Biochimica Et Biophysica Acta* **1958,** 28, (3), 464-469.

5.   Boldyrev, A. I.; Simons, J., Polyhedral ionic molecules. *Journal of the American Chemical Society* **1997,** 119, (20), 4618-4621.

6.   Hoffmann, R.; Lipscomb, W. N., Theory of Polyhedral Molecules .1. Physical Factorizations of Secular Equation. *Journal of Chemical Physics* **1962,** 36, (8), 2179.

7.   Drews, T.; Supel, J.; Hagenbach, A.; Seppelt, K., Solid state molecular structures of transition metal hexafluorides. *Inorganic Chemistry* **2006,** 45, (9), 3782-3788.

8.   Slee, T.; Lin, Z.; Mingos, D. M. P., Polyhedral skeletal electron pair theory of bare clusters. 1. Small silicon clusters. *Inorganic Chemistry* **1989,** 28, (12), 2256-2261.

9.   Toropova, K.; Basnak, G.; Twarock, R.; Stockley, P. G.; Ranson, N. A., The three-dimensional structure of genomic RNA in bacteriophage MS2: Implications for assembly. *Journal of Molecular Biology* **2008,** 375, (3), 824-836.

10.   Rossmann, M. G.; Johnson, J. E., Icosahedral RNA virus structure. *Annual Review of Biochemistry* **1989,** 58, (1), 533-569.

11.   Van der Spek, T. M., Selling a Theory: The Role of Molecular Models in JH van't Hoff's Stereochemistry Theory. *Annals of science* **2006,** 63, (02), 157-177.

12. Sachse, H., Ãœber die geometrischen Isomerien der Hexamethylenderivate. *Berichte der deutschen chemischen Gesellschaft* **1890,** 23, (1), 1363-1370.

13. Russell, C. A., Origins of Conformational-Analysis. *ACS Symposium Series* **1975**, (12), 159-178.

14. Eaton, P. E.; Cole, T. W., Cubane. *Journal of the American Chemical Society* **1964,** 86, (15), 3157-3158.

15. Paquette, L. A.; Ternansky, R. J.; Balogh, D. W.; Kentgen, G., Total synthesis of dodecahedrane. *Journal of the American Chemical Society* **1983,** 105, (16), 5446-5450.

16. Ternansky, R. J.; Balogh, D. W.; Paquette, L. A., Dodecahedrane. *Journal of the American Chemical Society* **1982,** 104, (16), 4503-4504.

17. Lewars, E., *Modeling marvels: computational anticipation of novel molecules*. Springer: 2008.

18. Maier, G. n.; Pfriem, S.; Schafer, U.; Matusch, R., Tetra□butyltetrahedrane. *Angewandte Chemie International Edition in English* **1978,** 17, (7), 520-521.

19. Chen, J.; Seeman, N. C., Synthesis from DNA of a molecule with the connectivity of a cube. *Nature* **1991,** 350, (6319), 631-633.

20. Zhang, Y.; Seeman, N. C., Construction of a DNA-truncated octahedron. *Journal of the American Chemical Society* **1994,** 116, (5), 1661-1669.

21. Zhang, C.; He, Y.; Su, M.; Ko, S. H.; Ye, T.; Leng, Y.; Sun, X.; Ribbe, A. E.; Jiang, W.; Mao, C., DNA self-assembly: from 2D to 3D. *Faraday discussions* **2009,** 143, 221-233.

22. Rothemund, P. W. K., Folding DNA to create nanoscale shapes and patterns. *Nature*

2006, 440, (7082), 297-302.

23.   Ebefors, T.; Kalvesten, E.; Stemme, G., New small radius joints based on thermal shrinkage of polyimide in V-grooves for robust self-assembly 3D microstructures. *Journal of Micromechanics and Microengineering* **1998,** 8, (3), 188-194.

24.   Smela, E.; Inganas, O.; Lundstrom, I., Controlled Folding of Micrometer-Size Structures. *Science* **1995,** 268, (5218), 1735-1738.

25.   Syms, R. R. A.; Yeatman, E. M., Self-Assembly of 3-Dimensional Microstructures Using Rotation by Surface-Tension Forces. *Electronics Letters* **1993,** 29, (8), 662-664.

26.   Syms, R. R. A., Rotational self-assembly of complex microstructures by the surface tension of glass. *Sensors and Actuators a-Physical* **1998,** 65, (2-3), 238-243.

27.   Vaccaro, P. O.; Kubota, K.; Aida, T., Strain-driven self-positioning of micromachined structures. *Applied Physics Letters* **2001,** 78, (19), 2852-2854.

28.   Gracias, D. H.; Kavthekar, V.; Love, J. C.; Paul, K. E.; Whitesides, G. M., Fabrication of micrometer-scale, patterned polyhedra by self-assembly. *Advanced Materials* **2002,** 14, (3), 235.

29.   Syms, R. R. A.; Yeatman, E. M.; Bright, V. M.; Whitesides, G. M., Surface tension-powered self-assembly of micro structures - The state-of-the-art. *Journal of Microelectromechanical Systems* **2003,** 12, (4), 387-417.

30.   Leong, T. G.; Zarafshar, A. M.; Gracias, D. H., Three-Dimensional Fabrication at Small Size Scales. *Small* **2010,** 6, (7), 792-806.

31.   Randall, C. L.; Gultepe, E.; Gracias, D. H., Self-folding devices and materials for biomedical applications. *Trends in Biotechnology* **2012,** 30, (3), 138-146.

32.   Gimi, B.; Leong, T.; Gu, Z. Y.; Yang, M.; Artemov, D.; Bhujwalla, Z. M.; Gracias, D.

H., Self-assembled three dimensional radio frequency (RF) shielded containers for cell encapsulation. *Biomedical Microdevices* **2005,** 7, (4), 341-345.

33. Cho, J. H.; Azam, A.; Gracias, D. H., Three Dimensional Nanofabrication Using Surface Forces. *Langmuir* **2010,** 26, (21), 16534-16539.

34. Pandey, S.; Ewing, M.; Kunas, A.; Nguyen, N.; Gracias, D. H.; Menon, G., Algorithmic design of self-folding polyhedra. *Proceedings of the National Academy of Sciences of the United States of America* **2011,** 108, (50), 19885-19890.

35. Cho, J. H.; Gracias, D. H., Self-Assembly of Lithographically Patterned Nanoparticles. *Nano Letters* **2009,** 9, (12), 4049-4052.

36. Azam, A.; Laflin, K. E.; Jamal, M.; Fernandes, R.; Gracias, D. H., Self-folding micropatterned polymeric containers. *Biomedical Microdevices* **2011,** 13, (1), 51-58.

37. Leong, T. G.; Lester, P. A.; Koh, T. L.; Call, E. K.; Gracias, D. H., Surface tension-driven self-folding polyhedra. *Langmuir* **2007,** 23, (17), 8747-8751.

38. Harsh, K.; Lee, Y. C., Modeling for solder self-assembled MEMS. *Micro-Optics Integration and Assemblies* **1998,** 3289, 177-184.

39. Syms, R. R. A., Equilibrium of hinged and hingeless structures rotated using surface tension forces. *Journal of Microelectromechanical Systems* **1995,** 4, (4), 177-184.

40. Harsh, K. F.; Bright, V. M.; Lee, Y. C., Solder self-assembly for three-dimensional microelectromechanical systems. *Sensors and Actuators a-Physical* **1999,** 77, (3), 237-244.

41. Randall, C. L.; Kalinin, Y. V.; Jamal, M.; Shah, A.; Gracias, D. H., Self-folding immunoprotective cell encapsulation devices. *Nanomedicine-Nanotechnology Biology and Medicine* **2011,** 7, (6), 686-689.

42.   Kalinin, Y. V.; Randhawa, J. S.; Gracias, D. H., Three-Dimensional Chemical Patterns for Cellular Self-Organization. *Angewandte Chemie-International Edition* **2011,** 50, (11), 2549-2553.

43.   Whitesides, G. M.; Grzybowski, B., Self-assembly at all scales. *Science* **2002,** 295, (5564), 2418-2421.

44.   Caspar, D. L. D., Citation Classic - Physical Principles in the Construction of Regular Viruses. *Current Contents/Life Sciences* **1984**, (4), 15-15.

45.   Lau, K. F.; Dill, K. A., A Lattice Statistical-Mechanics Model of the Conformational and Sequence-Spaces of Proteins. *Macromolecules* **1989,** 22, (10), 3986-3997.

46.   Chan, H. S.; Dill, K. A., The effects of internal constraints on the configurations of chain molecules (vol 92, pg 3118, 1990). *Journal of Chemical Physics* **1997,** 107, (23), 10353-10353.

47.   Chan, H. S.; Dill, K. A., The Effects of Internal Constraints on the Configurations of Chain Molecules. *Journal of Chemical Physics* **1990,** 92, (5), 3118-3135.

48.   Chen, J. H.; Seeman, N. C., Synthesis from DNA of a Molecule with the Connectivity of a Cube. *Nature* **1991,** 350, (6319), 631-633.

49.   Douglas, S. M.; Dietz, H.; Liedl, T.; Hogberg, B.; Graf, F.; Shih, W. M., Self-assembly of DNA into nanoscale three-dimensional shapes (vol 459, pg 414, 2009). *Nature* **2009,** 459, (7250), 1154-1154.

50.   He, Y.; Ye, T.; Su, M.; Zhang, C.; Ribbe, A. E.; Jiang, W.; Mao, C. D., Hierarchical self-assembly of DNA into symmetric supramolecular polyhedra. *Nature* **2008,** 452, (7184), 198-U41.

51.   Zimmermann, J.; Cebulla, M. R. J.; Monninghoff, S.; von Kiedrowski, G., Self-

assembly of a DNA dodecahedron from 20 trisoligonucleotides with C-3h linkers. *Angewandte Chemie-International Edition* **2008,** 47, (19), 3626-3630.

52.   Cromwell, P. R., Keplers Work on Polyhedra. *Mathematical Intelligencer* **1995,** 17, (3), 23-33.

53.   Shephard, G. C., Convex Polytopes with Convex Nets. *Mathematical Proceedings of the Cambridge Philosophical Society* **1975,** 78, (Nov), 389-403.

54.   Buekenhout, F.; Parker, M., The number of nets of the regular convex polytopes in dimension <= 4. *Discrete Mathematics* **1998,** 186, (1-3), 69-94.

55.   GrÃ¼nbaum, B.; Shephard, G. C., *Tilings and patterns*. Freeman: 1987.

56.   Wei, J., Molecular symmetry, rotational entropy, and elevated melting points. *Industrial & engineering chemistry research* **1999,** 38, (12), 5019-5027.

57.   Pines, H., *The chemistry of catalytic hydrocarbon conversions*. Elsevier.

58.   Somorjai, G. A.; Li, Y., *Introduction to surface chemistry and catalysis*. John Wiley & Sons.

59.   Jensen, H. J., *Self-organized criticality: emergent complex behavior in physical and biological systems*. Cambridge university press: 1998; Vol. 10.

60.   Chen, Y. Q.; Song, C.; Xiao, S. J.; You, X. Z., The programmable design and self-assembly of two-dimensional DNA crystals. *Chinese Journal of Inorganic Chemistry* **2005,** 21, (10), 1443-1449.

61.   Winfree, E.; Liu, F. R.; Wenzler, L. A.; Seeman, N. C., Design and self-assembly of two-dimensional DNA crystals. *Nature* **1998,** 394, (6693), 539-544.

62.   Colfen, H.; Mann, S., Higher-order organization by mesoscale self-assembly and transformation of hybrid nanostructures. *Angewandte Chemie-International Edition*

2003, 42, (21), 2350-2365.

63.   Rao, C. N. R., Porous materials: A case study of supramolecular organization in

materials design. *Bulletin of Materials Science* **1999,** 22, (3), 141-151.

64.   Gross, R.; Dorigo, M., Self-assembly at the macroscopic scale. *Proceedings of the*

IEEE **2008,** 96, (9), 1490-1508.

65.   Esch, J., Self-assembly at the macroscopic scale. *Proceedings of the Ieee* **2008,** 96, (9),

1487-1489.

66.   Park, S. H.; Xia, Y. N., Assembly of mesoscale particles over large areas and its

application in fabricating tunable optical filters. *Langmuir* **1999,** 15, (1), 266-273.

67.   Van der Spek, T. M., Selling a theory: The role of molecular models in J. H. van 't

Hoff's stereochemistry theory. *Annals of Science* **2006,** 63, (2), 157-177.

68.   Hsieh, D. S. T.; Rhine, W. D.; Langer, R., Zero-Order Controlled-Release Polymer

Matrices for Micromolecules and Macromolecules. *Journal of Pharmaceutical*

Sciences **1983,** 72, (1), 17-22.

69.   Euliss, L. E.; DuPont, J. A.; Gratton, S.; DeSimone, J. M., Imparting size, shape, and

composition control of materials for nanomedicine. *Chemical Society Reviews* **2006,**

35, (11), 1095-1104.

70.   Discher, D. E., Shape Effects of Filaments Versus Spherical Particles in Flow and

Drug Delivery. *Proceedings of the Asme Summer Bioengineering Conference 2008,*

Pts a and B **2009**, 739-739.

71.   Freiberg, S.; Zhu, X., Polymer microspheres for controlled drug release. *International*

Journal of Pharmaceutics **2004,** 282, (1-2), 1-18.

72.   Varde, N. K.; Pack, D. W., Microspheres for controlled release drug delivery. *Expert*

Opinion on Biological Therapy **2004,** 4, (1), 35-51.

73.   Bae, K. H.; Yoon, J. J.; Park, T. G., Fabrication of hyaluronic acid hydrogel beads for cell encapsulation. *Biotechnology Progress* **2006,** 22, (1), 297-302.

74.   Dang, S. M.; Kyba, M.; Perlingeiro, R.; Daley, G. Q.; Zandstra, P. W., Efficiency of embryoid body formation and hematopoietic development from embryonic stem cells in different culture systems. *Biotechnology and Bioengineering* **2002,** 78, (4), 442-453.

75.   Liu, V. A.; Bhatia, S. N., Three-dimensional photopatterning of hydrogels containing living cells. *Biomedical Microdevices* **2002,** 4, (4), 257-266.

76.   Khademhosseini, A.; Langer, R., Microengineered hydrogels for tissue engineering. *Biomaterials* **2007,** 28, (34), 5087-5092.

77.   Du, Y. A.; Lo, E.; Ali, S.; Khademhosseini, A., Directed assembly of cell-laden microgels for fabrication of 3D tissue constructs. *Proceedings of the National Academy of Sciences of the United States of America* **2008,** 105, (28), 9522-9527.

78.   Eppley, B. L.; Dadvand, B., Injectable Soft-Tissue Fillers: Clinical Overview. *Plastic and Reconstructive Surgery* **2006,** 118, (4), 98e-106e.

79.   Saralidze, K.; Knetsch, M. L. W.; van Hooy-Corstjens, C. S. J.; Koole, L. H., Radio-opaque and surface-functionalized polymer microparticles: Potentially safer biomaterials for different injection therapies. *Biomacromolecules* **2006,** 7, (11), 2991-2996.

80.   Dmochowski, R. R.; Appell, R. A., Injectable agents in the treatment of stress urinary incontinence in women: Where are we now? *Urology* **2000,** 56, (6A), 32-40.

81.   Mason, T. G.; Ganesan, K.; vanZanten, J. H.; Wirtz, D.; Kuo, S. C., Particle tracking microrheology of complex fluids. *Physical Review Letters* **1997,** 79, (17), 3282-3285.

82. Kim, S. H.; Abbaspourrad, A.; Weitz, D. A., Amphiphilic Crescent-Moon-Shaped Microparticles Formed by Selective Adsorption of Colloids. *Journal of the American Chemical Society* **2011,** 133, (14), 5516-5524.

83. Dinsmore, A. D.; Hsu, M. F.; Nikolaides, M. G.; Marquez, M.; Bausch, A. R.; Weitz, D. A., Colloidosomes: Selectively permeable capsules composed of colloidal particles. *Science* **2002,** 298, (5595), 1006-1009.

84. Yin, Y. D.; Xia, Y. N., Self-assembly of monodispersed spherical colloids into complex aggregates with well-defined sizes, shapes, and structures. *Advanced Materials* **2001,** 13, (4), 267-+.

85. El-Sayed, M. A., Small is different: Shape-, size-, and composition-dependent properties of some colloidal semiconductor nanocrystals. *Accounts of Chemical Research* **2004,** 37, (5), 326-333.

86. Kim, E.; Xia, Y. N.; Whitesides, G. M., Micromolding in capillaries: Applications in materials science. *Journal of the American Chemical Society* **1996,** 118, (24), 5722-5731.

87. Prebiotic, R. N. A., Polymer microstructures formed by moulding in capillaries. *Nature* **1995,** 376, 581.

88. Giboz, J.; Copponnex, T.; Mac, P., Microinjection molding of thermoplastic polymers: a review. *Journal of Micromechanics and Microengineering* **2007,** 17, (6), R96.

89. Zauner, R., Micro powder injection moulding. *Microelectronic engineering* **2006,** 83, (4), 1442-1444.

90. Sammoura, F.; Kang, J.; Heo, Y.-M.; Jung, T.; Lin, L., Polymeric microneedle

fabrication using a microinjection molding technique. *Microsystem technologies* **2007,** 13, (5-6), 517-522.

91. Vozzi, G.; Flaim, C.; Ahluwalia, A.; Bhatia, S., Fabrication of PLGA scaffolds using soft lithography and microsyringe deposition. *Biomaterials* **2003,** 24, (14), 2533-2540.

92. Xu, S.; Nie, Z.; Seo, M.; Lewis, P.; Kumacheva, E.; Stone, H. A.; Garstecki, P.; Weibel, D. B.; Gitlin, I.; Whitesides, G. M., Generation of monodisperse particles by using microfluidics: control over size, shape, and composition. *Angewandte Chemie* **2005,** 117, (5), 734-738.

93. Yeh, J.; Ling, Y. B.; Karp, J. M.; Gantz, J.; Chandawarkar, A.; Eng, G.; Blumling, J.; Langer, R.; Khademhosseini, A., Micromolding of shape-controlled, harvestable cell-laden hydrogels. *Biomaterials* **2006,** 27, (31), 5391-5398.

94. Champion, J. A.; Katare, Y. K.; Mitragotri, S., Making polymeric micro- and nanoparticles of complex shapes. *Proceedings of the National Academy of Sciences of the United States of America* **2007,** 104, (29), 11901-11904.

95. Franses, E. I.; Caruthers, J. M.; Keville, K. M., Nonspherical microparticles and method therefor. In Google Patents: 1988.

96. Hwang, D. K.; Dendukuri, D.; Doyle, P. S., Microfluidic-based synthesis of non-spherical magnetic hydrogel microparticles. *Lab on a Chip* **2008,** 8, (10), 1640-1647.

97. Dendukuri, D.; Tsoi, K.; Hatton, T. A.; Doyle, P. S., Controlled synthesis of nonspherical microparticles using microfluidics. *Langmuir* **2005,** 21, (6), 2113-2116.

98. Manoharan, V. N.; Elsesser, M. T.; Pine, D. J., Dense packing and symmetry in small clusters of microspheres. *Science* **2003,** 301, (5632), 483-487.

99. Yang, Y. Y.; Chung, T. S.; Ng, N. P., Morphology, drug distribution, and in vitro

release profiles of biodegradable polymeric microspheres containing protein fabricated by double-emulsion solvent extraction/evaporation method. *Biomaterials* **2001,** 22, (3), 231-241.

100. Kim, E.; Xia, Y.; Whitesides, G. M., Two and three□dimensional crystallization of polymeric microspheres by micromolding in capillaries. *Advanced Materials* **1996,** 8, (3), 245-247.

101. Mathiowitz, E.; Jacob, J. S.; Jong, Y. S.; Carino, G. P.; Chickering, D. E.; Chaturvedi, P.; Santos, C. A.; Vijayaraghavan, K.; Montgomery, S.; Bassett, M., Biologically erodable microspheres as potential oral drug delivery systems. *Nature* **1997,** 386, (6623), 410-414.

102. Lal, P.; Sun, W., Computer modeling approach for microsphere-packed bone scaffold. *Computer-Aided Design* **2004,** 36, (5), 487-497.

103. Borden, M.; Attawia, M.; Khan, Y.; Laurencin, C. T., Tissue engineered microsphere-based matrices for bone repair:: design and evaluation. *Biomaterials* **2002,** 23, (2), 551-559.

104. Champion, J. A.; Mitragotri, S., Role of target geometry in phagocytosis. *Proceedings of the National Academy of Sciences of the United States of America* **2006,** 103, (13), 4930-4934.

105. Champion, J. A.; Katare, Y. K.; Mitragotri, S., Particle shape: a new design parameter for micro-and nanoscale drug delivery carriers. *Journal of Controlled Release* **2007,** 121, (1), 3-9.

106. Fernandez, J. G.; Khademhosseini, A., Micro-Masonry: Construction of 3D Structures by Microscale Self-Assembly. *Advanced Materials* 22, (23), 2538-2541.

107.   Champion, J. A.; Walker, A.; Mitragotri, S., Role of particle size in phagocytosis of polymeric microspheres. *Pharmaceutical research* **2008,** 25, (8), 1815-1821.

108.   Doshi, N.; Mitragotri, S., Macrophages recognize size and shape of their targets. *PLoS One* 5, (4), e10051.

109.   Cho, M. S.; Cho, Y. H.; Choi, H. J.; Jhon, M. S., Synthesis and electrorheological characteristics of polyaniline-coated poly (methyl methacrylate) microsphere: size effect. *Langmuir* **2003,** 19, (14), 5875-5881.

110.   Mihi, A. n.; Oca, M.; MÃ-guez, H. n., Oriented Colloidal☐Crystal Thin Films by Spin Coating Microspheres Dispersed in Volatile Media. *Advanced Materials* **2006,** 18, (17), 2244-2249.

111.   Cho, Y.-S.; Yi, G.-R.; Lim, J.-M.; Kim, S.-H.; Manoharan, V. N.; Pine, D. J.; Yang, S.-M., Self-organization of bidisperse colloids in water droplets. *Journal of the American Chemical Society* **2005,** 127, (45), 15968-15975.

112.   Lumsdon, S. O.; Kaler, E. W.; Velev, O. D., Two-dimensional crystallization of microspheres by a coplanar AC electric field. *Langmuir* **2004,** 20, (6), 2108-2116.

113.   Yethiraj, A.; van Blaaderen, A., A colloidal model system with an interaction tunable from hard sphere to soft and dipolar. *Nature* **2003,** 421, (6922), 513-517.

114.   Randhawa, J. S.; Kanu, L. N.; Singh, G.; Gracias, D. H., Importance of Surface Patterns for Defect Mitigation in Three-Dimensional Self-Assembly. *Langmuir* **2010,** 26, (15), 12534-12539.

115.   Khademhosseini, A.; Langer, R.; Borenstein, J.; Vacanti, J. P., Microscale technologies for tissue engineering and biology. *Proceedings of the National Academy of Sciences of the United States of America* **2006,** 103, (8), 2480-2487.

116. Whitesides, G. M.; Ostuni, E.; Takayama, S.; Jiang, X. Y.; Ingber, D. E., Soft lithography in biology and biochemistry. *Annual Review of Biomedical Engineering* **2001,** 3, 335-373.

117. Bohr, M. T., Interconnect scaling - The real limiter to high performance ULSI. *International Electron Devices Meeting, 1995 - Iedm Technical Digest* **1995**, 241-244.

118. Bohr, M. T., Interconnect scaling - The real limiter to high performance ULSI. *Solid State Technology* **1996,** 39, (9), 105-&.

119. Loh, G. H.; Xie, Y.; Black, B., Processor design in 3D die-stacking technologies. *Ieee Micro* **2007,** 27, (3), 31-48.

120. Das, S.; Chandrakasan, A.; Reif, R. In *Three-dimensional integrated circuits: performance, design methodology, and CAD tools*, VLSI, 2003. Proceedings. IEEE Computer Society Annual Symposium on, 2003; IEEE: 2003; pp 13-18.

121. Das, S.; Fan, A.; Chen, K.-N.; Tan, C. S.; Checka, N.; Reif, R. In *Technology, performance, and computer-aided design of three-dimensional integrated circuits*, Proceedings of the 2004 international symposium on Physical design, 2004; ACM: 2004; pp 108-115.

122. Topol, A. W.; La Tulipe, D. C.; Shi, L.; Frank, D. J.; Bernstein, K.; Steen, S. E.; Kumar, A.; Singco, G. U.; Young, A. M.; Guarini, K. W., Three-dimensional integrated circuits. *IBM Journal of Research and Development* **2006,** 50, (4.5), 491-506.

123. Fan, A.; Rahman, A.; Reif, R., Copper wafer bonding. *Electrochemical and Solid State Letters* **1999,** 2, (10), 534-536.

124. Wong, S.; El-Gamal, A.; Griffin, P.; Nishi, Y.; Pease, F.; Plummer, J. In *Monolithic*

3D integrated circuits, VLSI Technology, Systems and Applications, 2007. VLSI-TSA 2007. International Symposium on, 2007; IEEE: 2007; pp 1-4.

125. Black, B.; Annavaram, M.; Brekelbaum, N.; DeVale, J.; Jiang, L.; Loh, G. H.; McCauley, D.; Morrow, P.; Nelson, D. W.; Pantuso, D. In *Die stacking (3D) microarchitecture*, Microarchitecture, 2006. MICRO-39. 39th Annual IEEE/ACM International Symposium on, 2006; IEEE: 2006; pp 469-479.

126. Gracias, D. H.; Tien, J.; Breen, T. L.; Hsu, C.; Whitesides, G. M., Forming electrical networks in three dimensions by self-assembly. *Science* **2000,** 289, (5482), 1170-1172.

127. Jacobs, H. O.; Tao, A. R.; Schwartz, A.; Gracias, D. H.; Whitesides, G. M., Fabrication of a cylindrical display by patterned assembly. *Science* **2002,** 296, (5566), 323-325.

128. Randhawa, J. S.; Gurbani, S. S.; Keung, M. D.; Demers, D. P.; Leahy-Hoppa, M. R.; Gracias, D. H., Three-dimensional surface current loops in terahertz responsive microarrays. *Applied Physics Letters* **2010,** 96, (19).

Shivendra Pandey

Department of Chemical and Biomolecular Engineering, The Johns Hopkins University
3400 N. Charles Street, 224 C MD Hall, Baltimore, MD 21218, USA
Email: shivendra@jhu.edu

I. Education

- Sep 2009- Sep 2014 **Ph.D**., Chemical and Biomolecular Engineering, **The Johns Hopkins University,** Baltimore, MD. Advisor: Prof. David H. Gracias

- Aug 2005- May 2009, **B. Tech.** Biotechnology, GPA: 8.8/10, **Indian Institute of Technology (IIT)** Guwahati, India.

II. Research and Teaching Experience

- Sep 2009 – Sep 2014, Graduate Research Assistant, Department of Chemical and Biomolecular Engineering, **Johns Hopkins University.**
- Sep 2011-Dec 2011, Teaching Assistant, Applied Physical Chemistry, Department of Chemical and Biomolecular Engineering, **Johns Hopkins University**.
- Jan 2010-May 2010, Teaching Assistant, Chemical Engineering Thermodynamics, Department of Chemical and Biomolecular Engineering, **Johns Hopkins University**.
- May 2008-Jul 2008, Visiting Undergraduate Researcher, Department of Materials Science and Engineering, **University of Florida**. Advisor: Prof. Henry Hess.
- Jun 2006- Jun 2009, Undergraduate Researcher, Department of Biotechnology and Center for Nanotechnology, **IIT Guwahati**, India. Advisors: Prof. Siddhartha Sankar Ghosh, Prof. Arun Chattopadhyay.

III. Skills and Expertise

- **Nano and Microfabrication:** Photolithography, Nanoimprint lithography, soft lithography, metallic and polymeric nanoparticles, quantum dots, self-assembly, vapor deposition, electroplating, thin-films, plasma etching, molding, MEMS, microfluidics, complex static and reconfigurable particles, self-assembled 3D computers.
- **Imaging:** SEM, AFM, STM, optical microscopy, fluorescence microscopy.
- **Characterization techniques:** DLS, XRD, UV-Vis and fluorescence spectrophotometry.
- **Simulation and software:** Monte-Carlo simulation, MATLAB, Mathematica and basic programming with C.
- **Vector programs:** AutoCAD, Autodesk Inventor.

IV. Peer Reviewed Publications

1. P. Sanpui, **S. Pandey**, S.S. Ghosh, A. Chattopadhyay, Green fluorescent protein for *in situ* synthesis of highly uniform Au nanoparticles and monitoring protein denaturation, ***Journal of Colloid and Interface Science***, 326, 1,129-37 (**2008).**

2. P. Sanpui[#], **S. Pandey**[#], A. Chattopadhyay, S.S. Ghosh, Incorporation of gene therapy vector in Chitosan stabilized Mn^{2+} doped ZnS Quantum Dots, ***Materials Letters***, 64, 2534-2537 (**2010**).
   { [#]*Contributed equally to this work.*}

3. I. Luria, J. Crenshaw, M. Downs, A. Agarwal, S. B. Seshadri, J.Gonzales, O. Idan, J. Kamcev, P. Katira, **S. Pandey**, T. Nitta, S. R. Phillpot, H. Hess, Microtubule nanospool formation by active self-assembly is not initiated by thermal activation, ***Soft Matter***, 7, 3108-3115 (**2011**).

4. **S. Pandey**, M. Ewing, A. Kunas, N. Nguyen, D. H. Gracias, G. Menon, Algorithmic design of self-folding polyhedra, ***Proceedings of the National Academy of Sciences of the United States of America (PNAS)*** 108, 50, 19885-19890 (**2011**).

5. **S. Pandey**, E. Gultepe, D. H. Gracias, Origami inspired self-assembly of patterned and reconfigurable particles, ***Journal of Visualized Experiments, 72, e50022*** (**2013**).

6. M. Karakoy, E. Gultepe**, S. Pandey,** M. Khashab and D. H. Gracias, Silane surface modification for improved bioadhesion of esophageal stents, ***Applied Surface Science*** (**2014**), accepted.

7. R. Kaplan[#], J. Klobusicky[#], **S. Pandey**[#] D. H. Gracias and G. Menon, Building polyhedra by self-assembly: Theory and experiments, (accepted) ***Artificial Life*** (**2014**). { [#]*Contributed equally to this work*}

8. **S. Pandey**, D. Johnson, R. Kaplan, J. Klobusicky, G. Menon and D. H. Gracias, Self- assembly of mesoscale isomers: The role of pathways and degrees of freedom, (accepted) ***PLOS One*** (**2014**).

V. Peer Reviewed Conference Papers:

1. J. Park, C. L. Randall, Y. V. Kalinin, **S. Pandey**, D. H. Gracias, A bio-artificial pancreas created using cell encapsulation in self-assembled microcontainers on an alginatesheet, *Proceedings of the 15th International Conference on Miniaturized Systems for Chemistry and Life Sciences (MicroTAS)*, 85-87, Seattle, WA (**2011**).

2. N. Macias, **S. Pandey**, A. Deswandikar, C. K. Kothapalli, C. K. Yoon, D.H. Gracias, C. Teuscher, A Cellular Architecture for Self-Assembled 3D Computational Devices, *IEEE/ACM International Symposium on Nanoscale Architechture (Nanoarch)*, NYC, (**2013**)

VI. Oral Presentations in Conferences:

1. **S. Pandey,** Z Zhilin, HR Kwag, CK Yoon, DH Gracias, Biologically inspired soft polyhedral, *MRS Meeting, Dec 1-6, 2013,* Boston.

2. **S. Pandey**, G. Menon, D.H. Gracias, Self-folding polyhedra and analogies to biomolecular assembly, *APS Meeting, Mar 18-22, 2013*, Baltimore

3. **S. Pandey**, J. S. Randhawa, D. H. Gracias, Three dimensional self-assembly using polyhedral building blocks, *ACS 86th Colloid and Surface Science Symposium, Jun 10-13, 2012*, Johns Hopkins University Baltimore.

4. **S. Pandey**, D. H. Gracias and G. Menon, Geometric principles for self-folding polyhedra: theory and experiments. *FNano 2012*, April 16-19, Snowbird, Utah.

5. **S. Pandey**, G. Menon and D. H. Gracias, Geometric considerations of nets for optimum self-folding of polyhedra, *MRS Direct self-assembly of materials Workshop, Sep 28, 2011*, Nashville.